Prepared for submission to JCAP

The Integrated Bispectrum and Beyond

Dipak Munshi[1], **Peter Coles**[2]

[1]Astronomy Centre, School of Mathematical and Physical Sciences,
University of Sussex, Brighton BN1 9QH, U.K.
[2]School of Physics and Astronomy, Cardiff University,
Queen's Buildings, The Parade, Cardiff CF24 3AA, U.K.

E-mail: D.Munshi@sussex.ac.uk, P.Coles@sussex.ac.uk

Abstract. The position-dependent power spectrum has been recently proposed as a descriptor of gravitationally induced non-Gaussianity in galaxy clustering, as it is sensitive to the "soft limit" of the bispectrum (i.e. when one of the wave number tends to zero). We generalise this concept to higher order and clarify their relationship to other known statistics such as the skew-spectrum, the kurt-spectra and their real-space counterparts the cumulants correlators. Using the *Hierarchical Ansatz* (HA) as a toy model for the higher order correlation hierarchy, we show how in the soft limit, polyspectra at a given order can be identified with lower order polyspectra with the same geometrical dependence but with *renormalised* amplitudes expressed in terms of amplitudes of the original polyspectra. We extend the concept of position-dependent bispectrum to bispectrum of the divergence of the velocity field Θ and mixed multispectra involving δ and Θ in the 3D perturbative regime. To quantify the effects of transients in numerical simulations, we also present results for lowest order in Lagrangian perturbation theory (LPT) or the Zel'dovich approximation (ZA). Finally, we discuss how to extend the position-dependent spectrum concept to encompass cross-spectra. And finally study the application of this concept to two dimensions (2D), for projected galaxy maps, convergence κ maps from weak-lensing surveys or maps of CMB secondaries e.g. the frequency cleaned y - parameter maps of thermal Sunyaev-Zel'dovich (tSZ) effect from CMB surveys.

Keywords: Cosmology, Large Scale Structure, Methods: analytical, statistical, numerical

Contents

1 Introduction **1**

2 Multispectra, Cumulant Correlators and the Large-Separation Limit **3**

3 Quasilinear Regime: Tree-level Results in the Soft (Squeezed) Limit **5**

4 Highly Non-linear Regime: Hierarchical *ansatz* (HA) in the Soft Limit **7**
4.1 Bispectrum in the soft limit 9
4.2 Trispectrum in the soft limit 10

5 Estimators for Polyspectra in their Soft Limit **11**
5.1 Estimator of the Squeezed Bispectrum 12
5.2 Estimators of Trispectrum: Squeezed and Collapsed 12

6 Integrated Bispectra: Quasilinar Regime **13**
6.1 A Unifying Approach 13
6.2 Mixed $\delta - \Theta$ Integrated Bispectra 16
6.3 Integrated Bispectra in Lagrangian Perturbation Theory 16

7 Integrated Bispectrum from Projected (2D) surveys **18**

8 Results and Discussion **20**

9 Acknowledgements **23**

A Perturbation Theory: A Very Brief Review **26**

B Perturbative Computation of the *Collapsed* Trispectrum **28**

C Perturbative Computation of *Squeezed* Trispectrum **30**
C.1 Squeezed-limit Trispectrum 31

1 Introduction

Over the last decade advances in astronomical spectroscopy and photometry of large samples of galaxies have allowed the galaxy distribution to be mapped to unprecedented accuracy and detail. Analysis of the resulting maps has yielded constraints on the growth rate of structures, expansion history of the Universe as well as on cosmological parameters. Examples include BOSS[1] [1] Wiggle[2] [2] DES[3] [3] and (the forthcoming) EUCLID[4] [4] In addition, the ongoing

[1]Baryon Oscillator Spectroscopic Survey: http://www.sdss3.org/surveys/boss.php
[2]Dark Energy Survey : http://wigglez.swin.edu.au/
[3]Dark Energy Survey: http://www.darkenergysurvey.org/
[4]EUCLID: http://www.euclid-ec.org/

and future Cosmic Microwave Background (CMB) missions such as Planck[5], ACT[6], and SPT[7] surveys will map the CMB sky with unprecedented resolution.

The successful measurement of cosmological parameters relies on both the accuracy of the theoretical models as well as the precision of the statistics used. In the past, the precision of the measurements was poor and a roughly 10% statistical error on the measurement of the power spectrum and even higher on the bispectrum was the limiting factor for discriminating among models and theories. However, current and forthcoming surveys are rapidly approaching the 1% statistical precision for two-point statistics, and are constraining higher-order statistics with similar level of improvement. This level of precision is comparable to the accuracy of the theoretical models that have been developed. In addition, the CMB sky at small angular scales is dominated by the secondaries, which are highly non-Gaussian as they trace the underlying large-scale structure. Consequently, a significant effort has been put into improving the theoretical development of new estimators for gravity induced non-Gaussianity. These include the optimal estimators such as the skew-$\mathcal{C}_\ell$ estimators [5] or the kurt-$\mathcal{C}_\ell$ estimators [6] as well as various sub-optimal morphological estimators [7].

Analytical understanding of gravitational clustering is generally based on four different approaches: (1) Standard petrurbative analysis of Euler-Continuity-Poisson system in the quasilinear regime [8] in Eulerian framework (SPT) or in Lagrangian space (LPT); (2) Physically motivated *ansatze* that capture certain aspects of gravitational clustering in the non-linear regime [31]; (3) effective field theory (EFT) based approaches [9]; and (4) halo model and its variants [10].

Gravity-induced higher-order correlation functions or their Fourier representations, the higher-order polyspectra, can provide important clues to structure formation scenarios (see Ref.[8] for a review). Measurements of the power spectrum in a sub-volume of the survey is statistically correlated with the average density contrast in that sub-volume. This correlation of this position power spectrum and the average density-contrast was recently used to define an estimator for the bispectrum in the *squeezed-limit* [11]. We will generalise the concept to position dependent power spectra to position-dependent angular polyspectra and show how such constructions can be used as estimators for higher-order polyspectra.

Cumulant correlators (CCs) are natural generalisation of one-point cumulants and provide an alternative route to study higher order correlation hierarchy and are well studied in the literature in the perturbative regime [12] and using hierarchical ansatz (HA) [13]. The Fourier representation of the lower-order CCs i.e. the skew-spectrum (third order)[5] and kurt-spectrum (fourth-order) [6] was also shown as an important form of data compression in 2D as well as in 3D. We derive the cumulant correlators in the large separation limit and study their relationship with the position-dependent multispectra hierarchy in the *soft* limit.

The organisation of the paper is as follows in §2 we discuss the Fourier transforms of the CCs; in §3 and §4 we derive the results for quasilinear and highly non-linear regime; the estimators for integrated bispectrum (IB) and integrated trispectrum (IT) are described in §5; the analytical expressions for bispectrum and trispectrum in squeezed limit are presented in §6 in a unified manner; in §7 we discuss the applications of these concepts to 2D (projected) surveys; the §8 is devoted to discussion of our results. We also present our conclusions and point out the future prospects in this section. Finally, in Appendices-§A, §B and §C we extend the idea of IB to IT.

[5]Planck: http://www.cosmos.esa.int/web/planck/
[6]ACT: http://www.physics.princeton.edu/act/
[7]SPT: http://pole.uchicago.edu/

We will concentrate on theoretical predictions in this paper. Comparison with numerical simulations and extensions to popular halo model based approach will be presented in future work. Observational aspects related to modelling of non-Gaussianities in CMB secondary maps or issues related to galaxy redshift space distortions will also be dealt with elsewhere.

For a discussion of the *soft* limits of polyspectra in the context of inflationary dynamics (see [14] and references there in). Certain aspects of the concept of polyspectra in the soft limit have been studied in the context of large-scale structure formation [15, 16]; comparison against numerical simulation was done in [17].

A note about our terminology is in order: by *polyspectra* we will mean the bispectrum, trispectrum and their higher-order analogs and with *multispectra* will mean derived statistics e.g. skew-spectrum, kurt-spectrum or their higher-order versions (optimal or sub-optimal). A polyspectra of n-th order is defined using n momenta denoted as $\mathbf{k}_i$.

[[The *soft limit* of a polyspectrum is reached when one or more of these momenta are much smaller than the others e.g. $k_1, \cdots, k_j \ll k_{j+1}, \cdots, k_n$ e.g. in case of the bispectrum the *squeezed* limit is reached when $k_1 \ll k_2, k_3$. In case of the trispectrum $k_1 \ll k_2, k_3, k_4$ defines the squeezed limit and $k_{12} \ll k_1, \cdots, k_4$; $k_{12} = |\mathbf{k}_1 + \mathbf{k}_2|$ defines the *collapsed* limit - both are special cases of the soft limit of the trispectrum.]]

2 Multispectra, Cumulant Correlators and the Large-Separation Limit

The use of multispectra has become widespread recently. The lowest order multispectrum (the skew-spectrum) probes the bispectrum [5]. Its fourth-order analogues are the kurt-spectra which probe the trispectrum [6]. In the following we will establish the link between these multispectra and their real-space analogs also known as the cumulant correlators [12]. This will allow us to express the multispectra of all order in the limit of large wavenumber k. Our aim is to elucidate the connection between the multispectra and the recently introduced integrated spectra.

The one-point cumulants $\langle \delta_s^p(\mathbf{x}) \rangle_c$ are collapsed multi-point correlation functions when all the p points are identified or collapsed to a single point; see, e.g., Ref.[8] for a review. The cumulants are typically employed for study of non-Gaussianity in many areas of cosmology including that of structure formation. The subscript "$_s$" indicates smoothing of the density contrast $\delta(\mathbf{x}) = (\rho(\mathbf{x}) - \bar{\rho})/\bar{\rho}$; where ρ is the density at a point $\mathbf{x}$ and $\bar{\rho}$ is the average density $\bar{\rho} \equiv \langle \rho(\mathbf{x}) \rangle$ of the Universe smoothed using a suitable smoothing window. The *normalised* cumulants $S_p = \langle \delta^p(\mathbf{x}) \rangle_c / \langle \delta^2(\mathbf{x}) \rangle_c^{p-1}$ are also used extensively in the literature; see Ref.[18] for analytical estimates.

The cumulant correlators (CC) are natural generalisations of the one-point cumulants to two-point statistics $\langle \delta_s^p(\mathbf{x}_1) \delta_s^p(\mathbf{x}_2) \rangle_c$ [12, 19, 20]. They are obtained by collapsing multipoint correlation functions of arbitrary order to two points. The normalised CCs denoted as C_{pq} are related to correlation function of order $(p+q)$ that are defined as [12]:

$$\langle \delta_s^p(\mathbf{x}_1) \delta_s^q(\mathbf{x}_2) \rangle_c \equiv \mathrm{C}_{pq} \, (\sigma_s^2)^{p+q-2}(R_0) \xi_{12}(\Delta x_{12}); \tag{2.1}$$

$$\xi_{12}(\Delta x_{12}) \equiv \langle \delta_s(\mathbf{x}_1) \delta_s(\mathbf{x}_2) \rangle_c; \quad \Delta x_{12} \equiv |\Delta \mathbf{x}_{12}| = |\mathbf{x}_1 - \mathbf{x}_2|. \tag{2.2}$$

$$\sigma_s^2 \equiv \langle \delta_s^2(\mathbf{x}) \rangle_c. \tag{2.3}$$

[[In general $\langle \delta_s^p(\mathbf{x}_1) \delta_s^q(\mathbf{x}_2) \rangle_c$ can depend on both position vectors $\mathbf{x}_1$ and $\mathbf{x}_2$ but statistical isotropy dictates that any such two-point statistics can depend only on the separation Δx_{12} as in Eq.(2.1) above.]] For a concrete example, consider the lowest order in the hierarchy of

CC, i.e. the two-to-one CC for a smoothed density contrast $\delta_i \equiv \delta_s(\mathbf{x}_i)$. We will be interested in the large separation limit $\Delta x_{12}/R_0 \gg 1$. This guarantees that we have $\Delta\xi_{12}/\sigma_s^2(R_0) \ll 1$; $\sigma_s^2(R_0)$ is the variance of the field obtained using a top-hat smoothing window $W_{\rm TH}(kR_0)$ (defined below) of radius R_0 as:

$$
\begin{aligned}
&S_{21}(\Delta x_{12}) \equiv \langle \delta_1^2 \delta_2 \rangle_c = \langle \delta_s^2(\mathbf{x}_1)\delta_s(\mathbf{x}_2)\rangle_c = \mathrm{C}_{21}\,\sigma_s^2\,\xi_{12}(\Delta x_{12}); \quad \Delta x_{12} = |\Delta \mathbf{x}_{12}|; \\
&\sigma_s^2(R_0) \equiv \int \frac{d^3k}{(2\pi)^3} W_{\rm TH}(kR_0) P(k); \\
&W_{\rm TH}(kR_0) \equiv \frac{3}{(kR_0)^3}\left[\sin(kR_0) - kR_0\cos(kR_0)\right].
\end{aligned}
\tag{2.4}
$$

Note we will use this form of smoothing throughout this paper. In length scales which are in the perturbative regime ($\sigma_s^2(R_0) \ll 1$ where tree-level results are valid) the normalised CCs typically become constant, as the loop-corrections from higher-order perturbation theory can safely be ignored in this limit. However, when $\sigma_s^2(R_0) \approx 1$, these corrections start to play an increasingly dominant role. The CC $\langle \delta_1^2\delta_2\rangle_c$ is obtained by identifying two of the points involved in a three-point correlation function $\langle \delta_1\delta_2\delta_3\rangle_c$, i.e $\mathbf{x}_1 \equiv \mathbf{x}_3$. It retains information regarding the three-point correlation function from which it is derived but only for a *collapsed* configuration. The Fourier-transform of Eq.(2.4) also known as *skew-spectrum* $S_{21}(k)$ in the large-separation limit:

$$
S_{21}(k') = \int \frac{d^3\Delta\mathbf{x}_{12}}{(2\pi)^3}\, S_{21}(x_{12})\exp[i\Delta\mathbf{x_{12}}\cdot\mathbf{k}']; \qquad k' = |\mathbf{k}'|. \tag{2.5}
$$

We will use the wave-number $\mathbf{k}'$ to represent the separation length-scale $\mathbf{x}_{12}$ and $\mathbf{k}$ to denote the smoothing scale R_0 above in the Fourier domain. We use the following expression $S_{21}(\Delta x_{12}) = \mathrm{C}_{21}\sigma_s^2\xi(\Delta x_{12})$ valid in the large separation limit $\Delta x_{12} \to \infty$ i.e $R_0/\Delta x_{12} \ll 1$:

$$
S_{21}(k') = \mathrm{C}_{21}\,\sigma_s^2(R_0)\,P(k'). \tag{2.6}
$$

The skew-spectrum in the Fourier domain, $S_{21}(k)$, represents the bispectrum in the squeezed limit. The power spectrum is defined through the Fourier-transform of the correlation function ξ_s:

$$
P(k') = \int \frac{d^3\Delta\mathbf{x}_{12}}{(2\pi)^3}\,\xi_s(\Delta x_{12})\exp[i\Delta\mathbf{x_{12}}\cdot\mathbf{k}']. \tag{2.7}
$$

The higher-order cumulant correlators $S_{pq}(x_{12})$ are natural generalisations of the two-to-one cumulant correlator defined above:

$$
S_{pq}(\Delta x_{12}) \equiv \langle \delta_1^p\delta_2^q\rangle_c = \langle \delta^p(\mathbf{x}_1)\delta^q(\mathbf{x}_2)\rangle_c = \mathrm{C}_{pq}\,\xi_{12}(\Delta x_{12})\,\sigma_s^{p+q-2}(R_0). \tag{2.8}
$$

The corresponding Fourier-transform defines the related collapsed multispectra $S_{pq}(k)$:

$$
S_{pq}(k') = \int \frac{d^3\Delta\mathbf{x}_{12}}{(2\pi)^3} S_{pq}(\Delta x_{12})\exp[i\Delta\mathbf{x_{12}}\cdot\mathbf{k}']. \tag{2.9}
$$

Using Eq.(2.8) in Eq.(2.9) we arrive at the following expression:

$$
S_{pq}(k') = \mathrm{C}_{pq}\,\sigma_s^{p+q-2}(R_0)\,P(k'). \tag{2.10}
$$

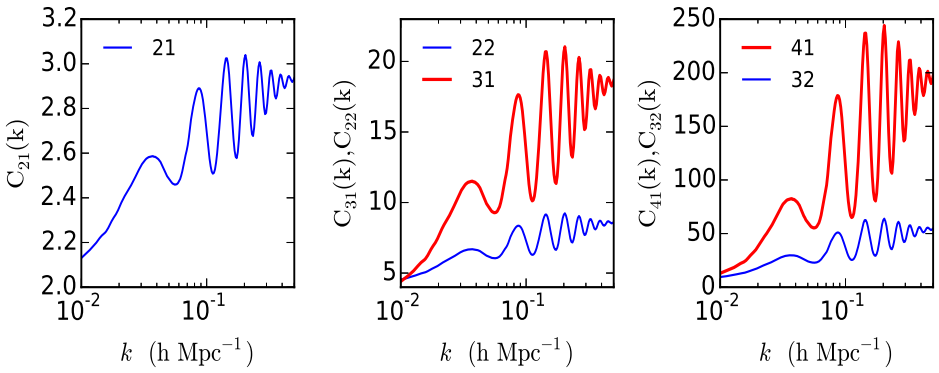

Figure 1: The 3D normalised cumulant corelators [defined in Eq.(3.4)-Eq.(3.5)] are plotted. The plots show $C_{21}(k)$ (left panel), $C_{31}(k)$ and $C_{22}(k)$ (middle panel) and $C_{41}(k)$ and $C_{32}(k)$ (right panel) as a function of the k wave number associated with the inverse of the radius of the top-hat smoothing window R_0. The results are derived using Standard Perturbation Theory (SPT) and the effective spectral index n was computed using the linear power spectrum.

The expressions for the lower order C_{pq} are given below in Eq.(3.4). Eq.(2.10) is the one of the important result of this paper. We will see that the position-dependent spectra we consider later in this paper have a structural similarity to the expressions for multispectra derived above in the above limit. We shall show that, for the bispectrum in the squeezed limit, the results are formally identical to the skew-spectrum at low k limit, though the mathematical interpretation is different. The normalised CC or C_{pq} are in general functions of the smoothing scale R_0 (equivalently the wavenumber k). The k dependence manifests itself as logarithmic slope n dependence of the power spectrum.

The lower-order CCs are plotted in Figure 1 as functions of $k\,(h^{-1}\mathrm{Mpc})$. We plot C_{21} (left-panel) C_{31} and C_{22} (middle-panel) and C_{41} and C_{32} (right-panel). The oscillations correspond to BAO signature in the underlying power spectrum. These plots depict the asymptotic value of the multispectra in the limit $k' \to 0$ as a function of k. In this limit the normalised CCs or C_{pq} are independent of k' and the k' dependence of S_{pq} is completely absorbed in $P(k')$. The C_{pq} are functions of local slope of the power spectrum.

3 Quasilinear Regime: Tree-level Results in the Soft (Squeezed) Limit

The quasilinear regime is defined through the relation $\sigma_s^2 < 1$. The two-point (joint) probability distribution function (PDF) for the smoothed (using a top-hat window) density field δ_s can be expressed in terms of the one-point $p_\delta(\delta)$, bias $b_\delta(\delta)$(defined below through Eq.(3.1)) in the large separation limit $\xi_{12}/\sigma_s^2 \ll 1$. Such a limiting situation is reached when the two cells are separated by a distance relatively larger than the smoothing scale.

$$p_\delta(\delta_1,\delta_2)d\delta_1 d\delta_2 = p_\delta(\delta_1)p_\delta(\delta_2)[\,1 + b_\delta(\delta_1)\,\xi_{12}^{\delta\delta}\,b_\delta\,(\delta_2)\,]d\delta_1 d\delta_2 \tag{3.1}$$

The CCs introduced in §2 are normalised two-point moments $\langle\delta_1^p\delta_2^q\rangle_c$ and can be expressed as:

$$\mathrm{C}_{pq}^{\delta\delta} \equiv \frac{\langle\delta_1^p\delta_2^q\rangle_c}{\langle\delta^2\rangle_c^{p+q-2}\langle\delta_1\delta_2\rangle_c}; \quad \langle\delta_1^p\delta_2^q\rangle_c = \int_{-1}^{\infty}\int_{-1}^{\infty}\delta_1^p\,\delta_2^q\,p(\delta_1,\delta_2)d\delta_1 d\delta_2. \tag{3.2}$$

By construction we have $\mathrm{C}_{11}^{\delta\delta} = 1$. In the large-separation limit the following factorisation property holds:

$$\mathrm{C}_{pq}^{\delta\delta} = \mathrm{C}_{p1}^{\delta\delta}\mathrm{C}_{q1}^{\delta\delta}. \tag{3.3}$$

In the quasilinear (perturbative) regime, the leading order terms of the entire hierarchy of C_{pq} can be evaluated analytically [12]. We quote here the following lower-order expressions:

$$\mathrm{C}_{21}^{\delta\delta} = \frac{68}{21} + \frac{\gamma_1}{3}; \tag{3.4}$$

$$\mathrm{C}_{31}^{\delta\delta} = \frac{11710}{441} + \frac{61}{7}\gamma_1 + \frac{2}{3}\gamma_1^2 + \frac{\gamma_2}{3}; \tag{3.5}$$

where the factors γ_p are defined as follows:

$$\gamma_p = \frac{\mathrm{d}^p\log\sigma^2(R_0)}{\mathrm{d}(\log R_0)^p}. \tag{3.6}$$

These results ignore contributions from loop diagrams and are thus valid only in the limiting situation when $\langle\delta^2\rangle \ll 1$. For power-law power spectra $P(k) \propto k^n$ we have $\gamma_1 = -(n+3)$ and $\gamma_p = 0$ for $p > 1$. In this limit the coefficients are polynomials in $n+3$, a property they share with the integrated spectra that we will study later. In case of the skew-spectra, the lowest order polynomial (i.e. linear) in this family, the coefficients match with those of the integrated bispectra (to be defined later) but this is not the case for higher order spectra. This is also true for the divergence of velocity Θ. For $n = -3$ these results represent statistics of unsmoothed fields and their values are determined completely by the angular averages of the tree-level amplitudes ν_n (see [25] for more discussion). In this limit they can be analysed by the HA (see §4). [[The angular averages of the tree-level amplitudes ν_n for δ defined in Eq.(A.8) and μ_n for Θ defined in Eq.(A.9) are discussed in Appendix-A. The recursion relation related to them are quoted in Eq.(A.15) and Eq.(A.16)]]

We will use the concept of C_{pq} for the case of velocity divergence $\Theta = -\nabla\cdot\mathbf{v}/H$ (to be introduced and discussed in more detail in §6) and generalise the concept of the integrated bispectrum to Θ. It is possible to consider mixed cumulant correlators of δ and Θ e.g. $\langle\delta_1^p\Theta_2^q\rangle$. In this case following similar arguments we can write:

$$\mathrm{C}_{pq}^{\delta\Theta} = \frac{\langle\delta_1^p\Theta_2^q\rangle_c}{\langle\delta_1^2\rangle^{p-1}\langle\Theta_2^2\rangle^{q-1}\langle\delta_1\Theta_2\rangle}; \tag{3.7}$$

$$\mathrm{C}_{pq}^{\delta\Theta} = \mathrm{C}_{p1}^{\delta\delta}\mathrm{C}_{q1}^{\Theta\Theta} \tag{3.8}$$

The corresponding joint PDF that generalises Eq.(3.1) is given by:

$$p_{\delta\Theta}(\delta_1,\Theta_2)d\delta_1 d\Theta_2 = p_\delta(\delta_1)p_\Theta(\Theta_2)[1 + b_\delta(\delta_1)\,\xi_{12}^{\delta\Theta}\,b_\Theta(\Theta_2)]d\delta_1 d\Theta_2. \tag{3.9}$$

Here, $p_{\delta\Theta}$ is the joint PDF for $\delta_1 \equiv \delta(\mathbf{x}_1)$ and $\Theta_2 \equiv \Theta(\mathbf{x}_2)$. The one-point PDFs for δ and Θ are denoted as $p_\delta(\delta)$ and $p_\Theta(\Theta)$. the corresponding bias functions are defined as b_δ and b_Θ respectively. The correlation function of δ and Θ is denoted $\xi_{12}^{\delta\Theta} \equiv \langle\delta_1\Theta_2\rangle$. In the Fourier domain we can similarly define mixed multispectra and their squeezed limits which can provide consistency checks on results obtained using δ and Θ fields alone.

4 Highly Non-linear Regime: Hierarchical *ansatz* (HA) in the Soft Limit

Gravity is scale-free. In the absence of of an externally-imposed length scale, such as might be set by initial conditions, it is reasonable to assume that gravitational clustering should evolve towards a scale-invariant form, at least on small scales (i.e. in the highly non-linear regime which is characterized by the $\sigma_s^2 \gg 1$.) where gravitational effect dominates over initial conditions [21–25]. Observations offer support for such an idea, in that the observed two-point correlation function $\xi_2(x)$ of galaxies is reasonably well represented by a power law over quite a large range of length scales, $\xi_2(r) \equiv \left(r/5h^{-1}\mathrm{Mpc}\right)^{-\gamma}$ between $100h^{-1}$ kpc and $10h^{-1}$Mpc. Higher-order correlation functions of galaxies also appear to satisfy a scale-invariant form, with $\xi_{\rm N} \propto \xi_2^{\rm N-1}$ as expected from the application of a general scaling *ansatz* [21, 22, 26]

For example, the observed lower-order correlation function exhibits a hierarchical form

$$\xi_{ab} \equiv \xi_2(\mathbf{x}_a, \mathbf{x}_b); \tag{4.1}$$

$$\xi_{abc} \equiv \xi_3(\mathbf{x}_a, \mathbf{x}_b, \mathbf{x}_c) \equiv \langle \delta(\mathbf{x}_a)\delta(\mathbf{x}_b)\delta(\mathbf{x}_c)\rangle_c = Q_3(\xi_{ab}\xi_{bc} + \xi_{bc}\xi_{ca} + \xi_{ab}\xi_{ac}); \tag{4.2}$$

$$\begin{aligned}\xi_{abcd} &\equiv \xi_4(\mathbf{x}_a, \mathbf{x}_b, \mathbf{x}_c, \mathbf{x}_d) \equiv \langle \delta(\mathbf{x}_a)\cdots\delta(\mathbf{x}_d)\rangle_c \\ &= R_a(\xi_{ab}\xi_{bc}\xi_{cd} + \text{cyc.perm.}) + R_b(\xi_{ab}\xi_{ac}\xi_{ad} + \text{cyc.perm.});\end{aligned} \tag{4.3}$$

$$\begin{aligned}\xi_{abcde} &\equiv \xi_5(\mathbf{x}_a, \cdots, \mathbf{x}_e) \equiv \langle \delta(\mathbf{x}_a)\cdots\delta(\mathbf{x}_e)\rangle_c \\ &= S_a(\xi_{ab}\xi_{bc}\xi_{cd}\xi_{de} + \text{cyc.perm.}) + S_b(\xi_{ab}\xi_{bc}\xi_{bd}\xi_{de} + \text{cyc.perm.}) \\ &+ S_c(\xi_{ab}\xi_{ac}\xi_{ad}\xi_{ae} + \text{cyc.perm.}).\end{aligned} \tag{4.4}$$

The hierarchy of equations - the Born, Bogolubov, Green, Kirkwood, Yvon (BBGKY) hierarchy that governs the evolution of the p-body density functions (in the full phase space) has been established for matter in an expanding universe [27]. Although the exact nature of this correlation hierarchy can only be obtained by solving the full set of BBGKY equations, which in general can not be done [21–23].

Useful insights can nevertheless be obtained by investigating the consequences of scaling properties to general closure [28, 29] schemes based fact that the hierarchy admits self-similar solutions [21]. The evolution of the power spectrum has also been tackled in a similar way [30]. In this approach the higher-order correlation functions can be expressed as:

$$\xi_{\rm N}(\mathbf{x}_1, \cdots, \mathbf{x}_{\rm N}) = \sum_{\alpha,\mathrm{N-trees}} Q_{N,\alpha} \sum_{\text{labelling edges}} \prod^{\rm N-1} \xi_2(\mathbf{x}_i, \mathbf{x}_j). \tag{4.5}$$

[[The above expression represents contribution from all possible *tree diagrmas* containing N-points. Different diagrams having the same topology are constructed by cyclic permutation of the vertices. All diagrmas with same topology correspond to the same amplitude $Q_{N,\alpha}$. Different edges in a diagram represent the corresponding two-point correlation functions.

Specific lower order cases of Eq.(4.5), e.g., for three-point, four-point and five-point correlation functions are given respectively in Eq.(4.2) - Eq.(4.4). These expressions are derived from Eq.(4.5) by following identifications: $Q_{3,1} = Q_3$, $Q_{4,1} = R_a$, $Q_{4,2} = R_b$ and $Q_{5,1} = S_a$, $Q_{5,2} = S_b$, $Q_{5,3} = S_c$. Note that there are no theoretical predictions for these topological amplitudes $Q_{N,\alpha}$ in this approach. Perturbative calculations have shown that gravity can induce a similar hierarchy starting from Gaussian initial conditions [23–25] in the limit of weak clustering. In a generic HA the topological amplitudes $[Q_3, R_a, R_b \cdots]$ are

left arbitrary. Specific HA models will be discussed later in this section. In the quasilinear regime these amplitudes can be computed using perturbative calculations.]]

This *tree-level* model of hierarchical clustering however is a particular case of a more general scaling ansatz proposed by [28], in which the N point correlation functions can be written in the form

$$\xi_{\rm N}(\lambda \mathbf{x}_1, \cdots, \lambda \mathbf{x}_{\rm N}) = \lambda^{\rm N-1} \xi_{\rm N}(\mathbf{x}_1, \cdots, \mathbf{x}_{\rm N}) \tag{4.6}$$

See, e.g., Ref.[31] and the reference therein. We shall work with the minimal hierarchical models as they distil some very basic features shared by other more complicated models. In the Fourier domain the equivalent results relate the higher-order polyspectra with the ordinary power sepctrum [20]. The bispectrum can be obtained by taking the Fourier transform of Eq.(4.2):

$$\langle \delta(\mathbf{k}_1)\delta(\mathbf{k}_2)\delta(\mathbf{k}_3)\rangle_c \equiv (2\pi)^3\, \delta_{\rm D}(\mathbf{k}_{123})\, B_2(\mathbf{k}_1, \mathbf{k}_2, \mathbf{k}_3); \tag{4.7}$$

$$B_2(\mathbf{k}_1, \mathbf{k}_2, \mathbf{k}_3) = Q_3 \left[P(k_1)P(k_2) + P(k_2)P(k_3) + P(k_1)P(k_3)\right]. \tag{4.8}$$

Throughout we will use $\mathbf{k}_{12\cdots p} = \mathbf{k}_1 + \mathbf{k}_2 + \cdots + \mathbf{k}_p$. The trispectrum $B_3(\mathbf{k}_1, \cdots, \mathbf{k}_4)$ is expressed in terms of two hierarchical amplitudes, R_a and R_b, introduced in Eq.(4.2):

$$\langle \delta(\mathbf{k}_1)\cdots\delta(\mathbf{k}_4)\rangle_c \equiv (2\pi)^3 \delta_D(\mathbf{k}_{1234}) B_3(\mathbf{k}_1, \cdots, \mathbf{k}_4) \tag{4.9}$$

$$\begin{aligned} B_3(\mathbf{k}_1, \cdots, \mathbf{k}_4) = {} & R_a \left[P(k_1)P(|\mathbf{k}_{12}|)P(|\mathbf{k}_{123}|) + \text{cyc.perm.}\right] \\ & + R_b [P(k_1)P(k_2)P(k_3) + \text{cyc.perm.}]. \end{aligned} \tag{4.10}$$

The next-order multispectrum $B_4(\mathbf{k_1}, \cdots, \mathbf{k_5})$ is obtained by taking FT of Eq.(4.3):

$$\langle \delta(\mathbf{k}_1)\cdots\delta(\mathbf{k}_5)\rangle_c \equiv (2\pi)^3 \delta_D(\mathbf{k}_{1234}) B_4(\mathbf{k}_1, \cdots, \mathbf{k}_5) \tag{4.11}$$

$$\begin{aligned} B_4(\mathbf{k_1}, \cdots, \mathbf{k_5}) = {} & S_a \Big[P(k_1)P(|\mathbf{k}_{12}|)P(|\mathbf{k}_{123}|)P(|\mathbf{k}_{1234}|) + \text{cyc.perm.}\Big] \\ & + S_b \left[P(k_1)P(k_2)P(|\mathbf{k}_{123}|)P(|\mathbf{k}_{1234}|) + \text{cyc.perm.}\right] \\ & + S_c \left[P(k_1)P(k_2)P(k_3)P(k_4) + \text{cyc.perm.}\right]. \end{aligned} \tag{4.12}$$

The result presented in Eq.(2.10) is derived using very general arguments. In the rest of this Section we will work out in detail for few specific models.

In the highly non-linear regime the higher-order correlation functions can be calculated using a hierarchical ansatz (HA) [13]. The parameters $\{Q_3\}$, $\{R_a, R_b\}$ and $\{S_a, S_b, S_c\}$ are topological amplitudes of various tree diagrams used to represent the correlation hierarchy at third fourth and fifth order, respectively. For specific models see Ref.[19, 28, 31, 32]. The lower-order linear combinations of these amplitudes that produce the one-point cumulants or S_N have been studied using numerical simulations [18].

In our calculation we will take the specific model by Bernardeau & Schaeffer [32] where we identify $Q_3 = \nu_2$, $R_a = \nu_2^2, R_b = \nu_3$ and $S_a = \nu_4, S_b = \nu_3\nu_2, S_c = \nu_2^3$. In the model proposed by Szapudi & Szalay [19] the tree amplitudes of a given order have identical values: $R_a = R_b$ and $S_a = S_b = S_c$ or in general in Eq.(4.5) $Q_{N,\alpha} = Q_N$.

In the quasilinear regime the vertices develop angular dependence on the wave vectors $\mathbf{k}_i$ (see Appendix-A for a brief review). In the tree-level perturbative regime the same tree hierarchy can be used and in the absence of smoothing the angular averaged biases can replace the corresponding ν_n s [23, 24]. The power spectrum in the quasilinear regime is

replaced by the linear power spectrum $P_{\rm L}(k)$. This is the regime we will use in this paper. We will omit the subscript $_L$ henceforth.

In the rest of the paper, we will use the HA developed by Bernardeau & Schaeffer discussed above [32].

4.1 Bispectrum in the soft limit

The influence of large-scale density fluctuations on structure formation results in the coupling of small and large-scale modes. At the lowest order such coupling can be described by the corresponding bispectrum in the so-called "squeezed" configuration. In the squeezed limit one of the wavenumbers, k_1, of the triangle representing the bispectrum in the Fourier domain, is much smaller than the other two i.e. $k_1 \ll k_2 \approx k_3$, thus, as we will see, effectively reducing the bispectrum to a power spectrum. In this limit the following parametrization applies:

$$B_2(\mathbf{k}-\mathbf{q_1},-\mathbf{k}+\mathbf{q_{12}},-\mathbf{q_2}) = Q_3\Big[P(|\mathbf{k}-\mathbf{q_1}|)P(|-\mathbf{k}+\mathbf{q_{12}}|) + P(|-\mathbf{k}+\mathbf{q_{12}}|)P(q_2) + P(|\mathbf{k}-\mathbf{q_2}|)P(q_2)\Big]. \tag{4.13}$$

The wavevectors $\mathbf{k}$ and $\mathbf{q}_i$ are independent. In this particular parametrization the squezzed limit can be taken in a transparent manner by taking the limit $q_i \to 0$. In our derivation, we will expand the power spectra in a Taylor-series as follows:

$$P(|\mathbf{k}-\mathbf{q_1}|) = P(k)\left[1-\frac{\mathbf{k}\cdot\mathbf{q_1}}{k^2}\frac{d\ln P(k)}{d\ln k}+\cdots\right]; \tag{4.14}$$

$$P(|-\mathbf{k}+\mathbf{q_{12}}|) = P(k)\left[1-\frac{\mathbf{k}\cdot\mathbf{q_{12}}}{k^2}\frac{d\ln P(k)}{d\ln k}+\cdots\right]. \tag{4.15}$$

Unlike the perturbative bispectrum, defined in Eq.(A.17), the hierarchical bispectrum, given in Eq.(4.8), does not display any Infrared (IR) divergence. In the squeezed limit $k \gg q_3$, so we ignore the terms of $\mathcal{O}(q_i/k)$ so that Eq.(4.13) takes the following form:

$$B_2(\mathbf{k}-\mathbf{q_1},-\mathbf{k}+\mathbf{q_{12}},-\mathbf{q_2}) \overset{\text{squeeze}}{\approx} 2Q_3P_L(q_2)P(k). \tag{4.16}$$

The corrections from the Taylor expansion in Eqs.(4.14-4.15) are only of $\mathcal{O}(q_i/k)^2$. Notice that we have also ignored terms of $\mathcal{O}[P(q_i)/P(k)]$ for CDM-like spectrum for $(q_i/k) \ll 1$. The subscript $_L$ denotes the linear power spectrum. The power spectrum is effectively in the linear regime for long wavemodes. This matches with the expression in Eq.(4.17). In the last term we have assumed for a CDM like spectrum $P(k) \ll P(q_2)$ for $k \gg q_3$. This is consistent with the result obtained in real space [20]:

$$\langle\delta_1^2\delta_2\rangle_c = \mathrm{C}_{21}\xi_{12}\sigma_L^2; \quad \mathrm{C}_{21} = 2Q_3. \tag{4.17}$$

The real space result can be obtained by identifying two of the points involved in a three-points $a = b$ and demanding $\xi_{ac} = \xi_{bc} \ll \xi_{ab}$ in Eq.(4.2) to neglect the linear order terms in ξ_{ac}/ξ_{aa} ($\xi_{aa} \equiv \sigma_L^2$).

In the specific model of Bernardeau & Schaeffer $Q_3 = \nu_2$. In the perturbative regime the unsmoothed results can be reproduced by taking $n = -3$ which gives $\nu_2 = 34/21$. Using this result we reproduce the result by Bernardeau in Ref.[12], i.e. $\mathrm{C}_{21} = 68/21$.

4.2 Trispectrum in the soft limit

In the soft limit the trispectrum can take either a *squeezed* or *collapsed* shape. In the squeezed case we have a configuration in which the trispectrum has one side much smaller than the others. In this configuration the trispectrum can be described effectively as a product of the bispectrum $B_2(\mathbf{k}_a, \mathbf{k}_b, \mathbf{k}_c)$ and the power spectrum $P(q)$; here $\mathbf{q}$ is the "soft" mode. We will use the following parametrization:

$$\begin{aligned} &B_3(\mathbf{k_a} - \mathbf{q_1}, \mathbf{k_b} - \mathbf{q_2}, \mathbf{k_c} + \mathbf{q_{123}}, -\mathbf{q_3}) \overset{\text{squeeze}}{=} \\ &R_a[P(q_3)\{P(k_a)P(k_b) + \text{cyc.perm.}\} + P(k_a)P(k_b)P(k_c)] \\ &+R_b[2P(q_3)\{P(k_a)P(k_b) + \text{cyc.perm.}\} + \{P(k_a)[P^2(k_b) + P^2(k_c)] + \text{cyc.perm.}\}] \end{aligned} \tag{4.18}$$

In the limit $k_a, k_b, k_c \gg q_3$ we have $P(k_a), P(k_b), P(k_c) \ll P(q_3)$, so the terms that survive are:

$$\begin{aligned} \lim_{\mathbf{q}_i \to 0} B_3(\mathbf{k_a} - \mathbf{q_1}, \mathbf{k_b} - \mathbf{q_2}, \mathbf{k_c} + \mathbf{q_{123}}, -\mathbf{q_3}) &\overset{\text{squeeze}}{\approx} \lim_{\mathbf{q}_3 \to 0} B_3(\mathbf{k_a}, \mathbf{k_b}, \mathbf{k_c}, -\mathbf{q_3}) \\ &\approx (R_a + 2R_b)P(q_3)[P(k_a)P(k_b) + \text{cyc.perm.}]\delta_{\rm D}(\mathbf{k}_{abc}). \end{aligned} \tag{4.19}$$

Both "snake" (terms with amplitude R_a) and "star" (terms with amplitude R_b) topologies contribute to the trispectrum in the squeezed limit. The effective bispectrum that describes the trispectrum in the squeezed limit has an amplitude $(R_a + 2R_b)$ rather than Q_3. For the other soft configuration we consider the case when one of the diameter of the quadrilateral representing the trispectrum is much smaller compared to its sides, also known as the collapsed configuration. In this configuration only the "snake" terms contribute:

$$\begin{aligned} \lim_{\mathbf{q} \to 0} B_3(\mathbf{k_1}, -\mathbf{k_1} - \mathbf{q}, \mathbf{k_2}, -\mathbf{k_2} + \mathbf{q}) &\overset{\text{collapsed}}{=} 2R_b \Big[2\,P(k_1)P(k_2)P(q) + 2\,P(k_1)P(|\mathbf{k_{12}}|)P(k_2) \\ &\quad + \left[P^2(k_1) + P^2(k_2)\right] P(|\mathbf{k_{12}}|) \Big]; \end{aligned} \tag{4.20}$$

$$B_3(\mathbf{k_1}, -\mathbf{k_1}, \mathbf{k_2}, -\mathbf{k_2}) \overset{\text{collapsed}}{\approx} 4R_b\, P(k_1)P(k_2)P(q). \tag{4.21}$$

In the collapsed configuration the trispectrum reduces to a product of three power spectra. The Fourier-space expressions Eq.(4.19) and Eq.(4.21) correspond respectively to Eq.(4.22) and Eq.(4.23) in real-space [20]:

$$\langle \delta_1^3 \delta_2 \rangle_c = \mathrm{C}_{31} \xi_{12} \sigma_L^4; \quad \mathrm{C}_{31} = (3R_a + 6R_b); \tag{4.22}$$

$$\langle \delta_1^2 \delta_2^2 \rangle_c = \mathrm{C}_{22} \xi_{12} \sigma_L^4; \quad \mathrm{C}_{22} = 4R_b. \tag{4.23}$$

Joint measurements of C_{31} and C_{22} can be used to estimate the amplitudes R_a and R_b: if we use $R_a \equiv \nu_3 = 682/189$ and $R_b \equiv \nu_2^2 = (34/21)^2$ we recover the result in [12] $\mathrm{C}_{31} = 11710/441$ and $\mathrm{C}_{22} = (68/21)^2$.

Here we note that previous studies have focused on many different aspects of such theories, including one-point probability distribution function, the void-probability distribution function and joint probability distribution function [28, 31, 32] which are directly related to the bias of over-dense objects [33]. Multi-point correlation function, cumulants and cumulant correlators of over-dense objects to arbitrary order have also been considered [13, 34–36]. The results presented here extend these results into the Fourier domain. We show how soft limits

of the polyspectra of arbitrary order can be studied by using local estimates of lower order polyspectra. [[The construction of soft limits in the perturbative regime to an arbitrary order is far more complicated. Indeed, the results from HA should only be considered only as an approximation as they are not valid in the limit of $k \to 0$ required to satisfy the inequality $k \ll k_i$. However, as with other statistics mentioned above the results using HA presented above provide valuable insights into the soft limit of higher order polyspectra.]]

5 Estimators for Polyspectra in their Soft Limit

In this Section we will develop a theory of the estimators for the squeezed multispectra. We will consider a density field $\delta(\mathbf{r})$ defined in a simulation box of side $L_{\rm box}$. We will also consider N^3 identical cubic sub-volumes with sides of length $L = L_{\rm box}/N$. The cosmological statistics measured in a sub-volume centred at the position r_L will be denoted L; the volume will be denoted $V_L = L^3$. To compute the squeezed higher-order multispectra we will cross-correlate the statistics measured in the entire simulation box against those estimated from these sub-volume. We will consider 3D surveys in this section but a generalisation to projected or 2D survey will be dealt with in §7. The results we present can be generalised to the case of observational data with minimal changes.

The local mean-density perturbations relative to the global mean density of the main volume is denoted as $\bar{\delta}(\mathbf{r}_L)$ and can be expressed through the following convolution:

$$\bar{\delta}(\mathbf{r}_L) = \frac{1}{V_L} \int d^3\mathbf{r}\, \delta(\mathbf{r})\, W_L(\mathbf{r} - \mathbf{r}_L). \tag{5.1}$$

The window function defined as $W_L(\mathbf{x}) \equiv \prod_{i=1}^{i=3} \theta(x_i)$. The one-dimensional unit step functions satisfy $\theta(x_i) = 1$ for $x_i \leq L/2$ and zero otherwise. The equivalent expression in the Fourier domain takes the following form:

$$\bar{\delta}(\mathbf{k}, \mathbf{r}_L) = \int \frac{d^3\mathbf{q}}{(2\pi)^3}\, \delta(\mathbf{k} - \mathbf{q})\, W_L(\mathbf{q}) \exp(-i\mathbf{r}_L \cdot \mathbf{q}) \tag{5.2}$$

The window W_L in the Fourier domain is given by:

$$W_L(\mathbf{q}) \equiv V_L \prod_i^3 \mathrm{sinc}\left[\frac{q_i\, L}{2}\right]; \tag{5.3}$$

where $\mathrm{sinc}(x) = \sin(x)/x$. The window has the following property which we will use throughout in our derivation:

$$W_L(\mathbf{r}) = W_L^2(\mathbf{r}); \quad W_L(\mathbf{q}_1) = \int \frac{d^3\mathbf{q}_2}{(2\pi)^3} W_L(\mathbf{q}_2) W_L(-\mathbf{q_{12}}). \tag{5.4}$$

The second identity can be proved using the *convolution* theorem.

The position dependent power spectrum $P(\mathbf{k}; \mathbf{r}_L) \equiv |\delta(\mathbf{k}; \mathbf{r}_L)|^2/V_L$ estimated from a sub-volume is given by the following expression:

$$P(\mathbf{k}; \mathbf{r}_L) = \frac{1}{V_L} \int \frac{d^3\mathbf{q}_1}{(2\pi)^3} \int \frac{d^3\mathbf{q}_2}{(2\pi)^3} \delta(\mathbf{k} - \mathbf{q}_1)\delta(-\mathbf{k} - \mathbf{q}_2) W_L(\mathbf{q}_1) W_L(\mathbf{q}_2). \tag{5.5}$$

This estimate of the local power spectrum can now be used to construct estimators for bispectrum and trispectrum in the soft limit.

5.1 Estimator of the Squeezed Bispectrum

The squeezed bispectrum can be estimated by cross-correlating the local estimates of the density contrast and the local power spectrum [11]:

$$\langle P(k)\bar{\delta}(\mathbf{r}_L)\rangle_c = \frac{1}{V_L^2}\int\frac{d^3\mathbf{q}_1}{(2\pi)^3}\cdots\int\frac{d^3\mathbf{q}_3}{(2\pi)^3}\langle\delta(\mathbf{k}-\mathbf{q_1})\delta(-\mathbf{k}-\mathbf{q_2})\delta(-\mathbf{q}_3)\rangle \times W_L(\mathbf{q}_1)W_L(\mathbf{q}_2)W_L(\mathbf{q}_3)\delta_{3\mathrm{D}}(\mathbf{q}_{123}). \tag{5.6}$$

Using Dirac δ_{3D} function to reduce the dimensionality of the above integral gives

$$\langle P(k)\bar{\delta}(\mathbf{r}_L)\rangle_c = \frac{1}{V_L^2}\int\frac{d^3\mathbf{q}_1}{(2\pi)^3}\int\frac{d^3\mathbf{q}_2}{(2\pi)^3}B_2[\mathbf{k}-\mathbf{q_1},-\mathbf{k}+\mathbf{q_{12}},-\mathbf{q_2}] \times W_L(\mathbf{q}_1)W_L(-\mathbf{q}_{12})W_L(\mathbf{q}_2). \tag{5.7}$$

$$\langle P(k)\bar{\delta}(\mathbf{r}_L)\rangle_c = 2Q_3\sigma_L^2P(k). \tag{5.8}$$

The derivation uses the result in Eq.(4.16). To arrive at the expression in Eq.(5.8) the second identity in Eq.(5.4) was used. This reduces the product of three window functions in Eq.(5.7) to $W_L^2(q_2)$, which is then absorbed in the definition of σ_L^2 given in Eq.(B.12).

In general the vertex Q_3 is defined in the Fourier space and carries an angular dependence. Integrating out this dependence gives the integrated bispectrum $\bar{\mathcal{B}}_{21}$:

$$\mathcal{B}_{21}(\mathbf{k},r_L) = \langle P(\mathbf{k},r_L)\bar{\delta}(r_L)\rangle_c; \quad \bar{\mathcal{B}}_{21}(k) \equiv \int\frac{d\hat{\Omega}_k}{4\pi}\mathcal{B}_{21}(\mathbf{k},r_L). \tag{5.9}$$

5.2 Estimators of Trispectrum: Squeezed and Collapsed

As we have previously mentioned, in the soft limit the trispectrum B_3 exists in *squeezed* and *collapsed* configuration, which we discuss next. We will show that trispectrum in the squeezed limit can be constructed by correlating the local estimates of the bispectrum B_2 and the local average density contrast $\bar{\delta}$. The collapsed limit of the trispectrum is constructed using covariance matrix for the local power spectrum.

Squeezed: Local estimates of the bispectrum from a small patch of a survey and the average density contrast measured from the same patch are correlated. The correlation is a measure of the trispectrum in the squeezed limit described in Eq.(4.18):

$$\begin{aligned}\langle B_2\bar{\delta}(\mathbf{r}_L)\rangle_c &\equiv \langle B_2(\mathbf{k_a},\mathbf{k_b},\mathbf{k_c};r_L)\bar{\delta}(\mathbf{r}_L)\rangle_c \\ &= \frac{1}{V_L^2}\int\frac{d^3\mathbf{q}_1}{(2\pi)^3}\cdots\int\frac{d^3\mathbf{q}_4}{(2\pi)^3}\langle\delta(\mathbf{k_a}-\mathbf{q_1})\delta(\mathbf{k_b}-\mathbf{q_2})\delta(\mathbf{k_c}-\mathbf{q_3})\delta(-\mathbf{q}_4)\rangle \\ &\quad\times W_L(\mathbf{q}_1)W_L(\mathbf{q}_2)W_L(\mathbf{q}_3)W_L(\mathbf{q}_4)\,\delta_{\mathrm{D}}(\mathbf{q}_{1234})\delta_{\mathrm{D}}(\mathbf{k}_{abc}).\end{aligned} \tag{5.10}$$

Integrating out the variable $\mathbf{q}_4$ collapses the above 4D integral to a 3D integral:

$$\langle B_2\bar{\delta}(\mathbf{r}_L)\rangle_c = \frac{1}{V_L^2}\int\frac{d^3\mathbf{q}_1}{(2\pi)^3}\cdots\int\frac{d^3\mathbf{q}_3}{(2\pi)^3}B_3[\mathbf{k_a}-\mathbf{q_1},\mathbf{k_b}-\mathbf{q_2},\mathbf{k_c}+\mathbf{q_{123}},-\mathbf{q_3}] W_L(\mathbf{q}_1)W_L(\mathbf{q}_2)W_L(-\mathbf{q}_{123})W_L(\mathbf{q}_3). \tag{5.11}$$

$$\mathcal{T}_{31}(\mathbf{k}_a,\mathbf{k}_b,\mathbf{k}_c) \equiv \langle B_2\bar{\delta}(\mathbf{r}_L)\rangle_c = (R_a+2R_b)\sigma_L^2[P(k_a)P(k_b)+\text{cyc.perm.}]. \tag{5.12}$$

We have used the expression in Eq.(4.18) for our derivation. Repeated use of the Eq.(5.4) simplified the expressions involving the window functions.

Table 1: Approximations and Kernels

SPT	Standard Perturbation Theory	F_n Eq.(A.3) G_n Eq.(A.4) F_2 Eq.(A.10) G_2 Eq.(A.12)
LPT	Lagrangian Perturbation Theory	
ZA	Zeldovich Approximation	$F_n^{\rm ZA}$ Eq.(A.7)
HA	Hierarchical Ansatz	Eq.(4.1-4.3); Eq.(4.8-4.12)

Collapsed: For the other "soft" configuration the sides of the quadrangle are much bigger compared to one of its diagonal. We have ignored the terms that are of $\mathcal{O}(q/k_i)$. This is the Fourier analogue of the expression in Eq.(4.23):

$$\langle P(\mathbf{k}_a,\mathbf{r}_L)P(\mathbf{k}_b,\mathbf{r}_L)\rangle_c = \delta_D(\mathbf{k}_{12})\frac{1}{V_L^2}\int\frac{d^3\mathbf{q}_1}{(2\pi)^3}\int\frac{d^2\mathbf{q}_2}{(2\pi)^3}B_3(-\mathbf{k}_a,\mathbf{k}_a-\mathbf{q}_1,\mathbf{k}_b,\mathbf{k}_b-\mathbf{q}_2)$$
$$\times W_L(\mathbf{q}_1)W_L(\mathbf{q}_2) \tag{5.13}$$
$$\mathcal{T}_{22}(\mathbf{k}_1,\mathbf{k}_2) = \langle P(\mathbf{k}_a)P(\mathbf{k}_b,\mathbf{r}_L)\rangle_c = 4\,R_b\,P(k_a)\,P(k_b)\sigma_L^2\delta_D(k_{12}). \tag{5.14}$$

Eq.(5.14) is an estimate of the covariance of the local power spectrum. We have used Eq.(4.21) and Eq.(5.4) in our derivation.

To define the integrated trispectra we can integrate the angular dependence of the vertices R_a and R_b in the Fourier space in a way similar to the bispectrum case.

The integrated trispectra $\mathcal{T}_{31}(\mathbf{k}_a,\mathbf{k}_b,\mathbf{k}_c)$ and $\mathcal{T}_{22}(\mathbf{k}_a,\mathbf{k}_b)$ defined in Eq.(5.8) and Eq.(5.14) are related to the kurt-spectra i.e. S_{31} and S_{22} discussed previously.

6 Integrated Bispectra: Quasilinar Regime

In this section we will provide a unifying description of the integrated bispectrum in various specific cases, e.g. the case of Standard Perturbation Theory(SPT) description of density contrast δ velocity divergence Θ, 2D dynamics and the Zel'dovich approximation (ZA).

6.1 A Unifying Approach

[[In aperturbative analysis the density contrast δ and the velocity divergence $\Theta = \nabla\cdot\mathbf{v}/H$ (H is the Hubble parameter) are expanded in a perturbative series Eq.(A.1)-Eq.(A.2). The $n^{\rm th}$ order terms $\delta^{(n)}$ and $\Theta^{(n)}$ can be expressed through a convolution using kernels $F^{(n)}$ and $G^{(n)}$. The second order kernels $F^{(2)}(\mathbf{k}_1,\mathbf{k}_2)$ and $G^{(2)}(\mathbf{k}_1,\mathbf{k}_2)$ are given in Eq.(A.10) and Eq.(A.12). The perturbative kernels $F_n^{\rm ZA}$ for Zeldovich Approximation are given in Eq.(A.7). For detailed derivation of these kernels see Ref.[8]. In Table-1 pointers to the various equations defining the kernels are presented. The estimators are listed in Table-2.

Table 2: Estimators

CCs	-
Pure	Eq.(2.1)
Minxed	Eq.(3.7)
Multispectra	Eq.(2.10)
3D δ IB (PT)	Eq.(6.8)
3D Θ IB (PT)	Eq.(6.9)
3D Mixed IB (PT)	Eq.(6.14)
2D δ IB (PT)	Eq.(6.10)
2D Θ IB (PT)	Eq.(6.11)
3D δ IB (HA)	Eq.(4.16)
3D IT (PT)	-
$\mathrm{B}^{\mathrm{coll}}$	Eq.(B.12)
B^{sq}	Eq.(C.18)
IT (HA)	-
$\mathcal{B}_{31}$	Eq.(4.19)
$\mathcal{B}_{22}$	Eq.(4.21)

The kernel $X_2(\mathbf{k}_1, \mathbf{k}_2)$ defined below represents both $F_2(\mathbf{k}_1, \mathbf{k}_2)$, $F_2^{\mathrm{ZA}}(\mathbf{k}_1, \mathbf{k}_2)$ and $G_2(\mathbf{k}_1, \mathbf{k}_2)$ for different values of the parameters of α and β:]]

$$X_2(\mathbf{k}_1, \mathbf{k}_2) = \alpha + \frac{1}{2}(\alpha+\beta)\left(\frac{k_1}{k_2}+\frac{k_2}{k_1}\right)\left(\frac{\mathbf{k}_1\cdot\mathbf{k}_2}{k_1k_2}\right) + \beta\left(\frac{\mathbf{k}_1\cdot\mathbf{k}_2}{k_1k_2}\right)^2. \tag{6.1}$$

The above parametrization satisfies the constraint $X_2(\mathbf{k}, -\mathbf{k}) = 0$ from momentum conservation (translational invariance) [37]. We have kept α and β free but all physical models that we will consider satisfy $(\alpha+\beta) = 1$.

$$\begin{aligned} X_2(\mathbf{k}-\mathbf{q}_1, -\mathbf{q}_3) &\approx \alpha + \frac{1}{2\,(kq_3)^2}(\alpha+\beta)\left[-(\mathbf{k}\cdot\mathbf{q_3})k^2 + (\mathbf{q}_1\cdot\mathbf{q}_3)k^2\right] + \beta\left(\frac{\mathbf{k}\cdot\mathbf{q}_3}{kq_3}\right)^2; \\ X_2(-\mathbf{k}+\mathbf{q}_{13}, -\mathbf{q}_3) &\approx \alpha + \frac{1}{2(kq_3)^2}(\alpha+\beta)\left[k^2(\mathbf{k}\cdot\mathbf{q_3}) - k^2(\mathbf{q}_1\cdot\mathbf{q}_{13})\right] + \beta\left(\frac{\mathbf{k}\cdot\mathbf{q}_3}{kq_3}\right)^2. \end{aligned} \tag{6.2}$$

The bispectrum B_2 corresponding to the kernel X_2 can be constructed using the Eq.(A.17), by replacing F_2 with X_2.

Imposing $\alpha+\beta = 1$, the result for the squeezed bispectrum takes the following form:

$$\begin{aligned} &B_2(\mathbf{k}-\mathbf{q}_1, -\mathbf{k}+\mathbf{q}_{13}, -\mathbf{k}_3) \\ &\qquad = \left\{(3\alpha-\beta) + 4\beta\left(\frac{\mathbf{k}\cdot\mathbf{q}_3}{kq_3}\right)^2 - (\alpha+\beta)\left(\frac{\mathbf{k}\cdot\mathbf{q}_3}{kq_3}\right)^2\frac{d\ln P(k)}{d\ln k}\right\}P(k)P(q_3); \quad (6.3) \\ &= \left[3\alpha + \frac{\beta}{3} + 1 - \frac{1}{3}\frac{d\ln k^3P(k)}{d\ln k}\right]P(k)P(q_3) \quad (\text{for } 3\mathrm{D}); \quad (6.4) \\ &= \left[3\alpha + \beta + 1 - \frac{1}{2}\frac{d\ln k^2P(k_\perp)}{d\ln k_\perp}\right]P(k_\perp)P(q_{\perp 3}) \quad (\text{for } 2\mathrm{D}). \quad (6.5) \end{aligned}$$

The specific cases so far we have analysed in this paper are examples where the triplets $\{\alpha, \beta\}$ take the following values $\{5/7, 2/7\}$ for SPT (Standard Perturbation Theory) $\{1/2, , 1/2\}$ for ZA and $\{3/7, 4/7\}$ for velocity divergence Θ. For projected density fields the angular averages need to be considered in 2D. The actual bispectrum remains the same as 3D.

More complicated kernel where the parameters α, β are redshift z and mode k dependent provides better fit to numerical simulations and has also been considered in the literature which can be incorporated in this framework.

For a generic cosmology the kernels take the following form Ref.[12] (see Eq.(71) and Eq.(72) of this review Ref.[12] (Section:2.4.5); we have corrected a typo in Eq.(71)):

$$F_2(\mathbf{k}_1, \mathbf{k}_2) = \frac{1}{2}(1+\epsilon) + \frac{1}{2}\left(\frac{k_1}{k_2} + \frac{k_2}{k_1}\right)\left(\frac{\mathbf{k}_1 \cdot \mathbf{k}_2}{k_1 k_2}\right) + \frac{1}{2}(1-\epsilon)\left(\frac{\mathbf{k}_1 \cdot \mathbf{k}_2}{k_1 k_2}\right)^2; \tag{6.6}$$

$$G_2(\mathbf{k}_1, \mathbf{k}_2) = \epsilon + \frac{1}{2}\left(\frac{k_1}{k_2} + \frac{k_2}{k_1}\right)\left(\frac{\mathbf{k}_1 \cdot \mathbf{k}_2}{k_1 k_2}\right) + (1-\epsilon)\left(\frac{\mathbf{k}_1 \cdot \mathbf{k}_2}{k_1 k_2}\right)^2. \tag{6.7}$$

The F_2 and G_2 as explained above are special cases of X_2 defined in Eq.(6.2). The perturbative bispectrum for δ can be constructed from F_2 using Eq.(A.17) and similarly for Θ using G_2 instead. Here, $\epsilon = 3/7\Omega_{\rm M}^{-2/63}$ for $\Omega_{\rm M} \geq 0.1$ Ref.[38]. The parameter ϵ does not represent any physical quantity. It is used here to derive results for arbitrary $\Omega_{\rm M}$. In this parametrization the kernel $F_2^{\rm ZA}$ in Eq.(6.17) can be recovered using $\epsilon = 0$. Using the generic expressions above in Eq.(6.1) we arrive at the following results for 3D:

$$\bar{\mathcal{B}}^{\delta}(k) = \frac{1}{3}\left[(8+4\epsilon) - (n+3)\right]\sigma_L^2 P_\delta(k); \tag{6.8}$$

$$\bar{\mathcal{B}}^{\Theta}(k) = \frac{1}{3} f^3(\Omega)\left[(4+8\epsilon) - (n+3)\right]\sigma_L^2 P_\delta(k). \tag{6.9}$$

For $\Omega_{\rm M} = 1$ we recover $\bar{\mathcal{B}}^{\delta}(k) \equiv [68/21 - (n+3)/3]$ and $\bar{\mathcal{B}}^{\Theta}(k) \equiv [52/21 - (n+3)/3]$. For all practical purposed these results are sufficient as the dependence on Ω_M is is extremely weak. For ZA we have $\bar{\mathcal{B}}^{\rm ZA,\delta}(k) \equiv [8/3 - (n+3)/3]$ and $\bar{\mathcal{B}}^{\rm ZA,\Theta}(k) \equiv [4/3 - (n+3)/3]$. In case of $n = -3$ we recover the unsmoothed values $\bar{\mathcal{B}}^{\delta}(k) = 2\nu_2 = 68/21$ and $\bar{\mathcal{B}}^{\Theta}(k) = 2\mu_2 = 52/21$. In comparison the skewness parameters are given by $S_3^{\delta} \equiv 3\nu_2$ and $S_3^{\Theta} = 3\mu_2$. In 2D we have the following results:

$$\bar{\mathcal{B}}^{\delta}_{2D}(k) = \left[(2+\epsilon) - \frac{1}{2}(n+2)\right]\sigma_L^2 P_\delta(k_\perp); \tag{6.10}$$

$$\bar{\mathcal{B}}^{\Theta}_{2D}(k) = f^3(\hat{\Omega})\left[(2\epsilon+2) - \frac{1}{2}(n+2)\right]\sigma_L^2 P_\delta(k_\perp). \tag{6.11}$$

For $\Omega = 1$ we recover $\bar{\mathcal{B}}^{\delta}(k) = [(24/7) - (n+2)/2]\sigma^2_{\rm 2D,L} P_\delta(k_\perp)$.

To linear order we have the well known result: $\Theta = -f(\Omega)\delta$. Using this in Eq.(6.9) we obtain:

$$\bar{\mathcal{B}}^{\Theta}(k) = -\frac{1}{3\,f(\Omega)}\left[(4+8\epsilon) - (n+3)\right]\sigma^2_{\Theta L} P_\Theta(k). \tag{6.12}$$

Here, $f(\Omega) \approx \Omega^{3/5}$. This function is sensitive to any variation of Ω which makes the integrated bispectrum of Θ sensitive to Ω, in contrast to δ.

6.2 Mixed $\delta - \Theta$ Integrated Bispectra

In our analysis so far we have cross correlated the $\bar{\delta}$ and $P_\delta(k)$ as well as $\bar{\Theta}$ and $P_\Theta(k)$; these probe the squeezed *pure* bispectrum i.e. $B_{\delta\delta\delta}$ or $B_{\Theta\Theta\Theta}$ but it is possible to device consistency tests by considering the mixed bispectra $B_{\delta\Theta\Theta}$ or $B_{\Theta\delta\delta}$.

Generalising Eq.(5.8) we introduce the following pair of mixed bispectra:

$$\begin{aligned}\langle P_{\delta\delta}(k)\bar{\Theta}(\mathbf{r}_L)\rangle_c = & \frac{1}{V_L^2}\int\frac{d^3\mathbf{q}_1}{(2\pi)^3}\int\frac{d^3\mathbf{q}_2}{(2\pi)^3}B_{\delta\delta\Theta}[\mathbf{k}-\mathbf{q_1},-\mathbf{k}+\mathbf{q_{12}},-\mathbf{q_2}] \\ & \times W_L(\mathbf{q}_1)W_L(-\mathbf{q}_{12})W_L(-\mathbf{q}_2); \qquad (6.13)\\ \langle P_{\Theta\Theta}(k)\bar{\delta}(\mathbf{r}_L)\rangle_c = & \frac{1}{V_L^2}\int\frac{d^3\mathbf{q}_1}{(2\pi)^3}\int\frac{d^3\mathbf{q}_2}{(2\pi)^3}B_{\Theta\Theta\delta}[\mathbf{k}-\mathbf{q_1},-\mathbf{k}+\mathbf{q_{12}},-\mathbf{q_2}] \\ & \times W_L(\mathbf{q}_1)W_L(-\mathbf{q}_{12})W_L(-\mathbf{q}_2). \qquad (6.14)\end{aligned}$$

Going through the same algebra we can show:

$$\langle P_{\delta\delta}(k)\bar{\Theta}(\mathbf{r}_L)\rangle_c = f(\Omega)\left[\frac{68}{21}-\frac{n+3}{3}\right]\sigma_L^2 P_\delta(k); \qquad (6.15)$$

$$\langle P_{\Theta\Theta}(k)\bar{\delta}(\mathbf{r}_L)\rangle_c = -f^2(\Omega)\left[\frac{52}{21}-\frac{n+3}{3}\right]\sigma_L^2 P_\delta(k). \qquad (6.16)$$

Both expressions are sensitive to Ω owing to the presence of Θ. Notice that the power spectra and the variance in these expressions are for δ unlike in Eq.(6.12) where it was for Θ.

Standard (Eulerian) Perturbation Theory (SPT) is known to agree well with numerical simulations for $z \geq 1$ and $k \leq 0.2\text{hMpc}^{-1}$. They fail to provide accurate results in the highly non-linear regime e.g. for the Baryon Acoustic Oscillation (BAOs) amplitudes at $k \geq 0.2\text{hMpc}^{-1}$. The SPT predictions are redshift-independent, though in simulations BAOs show smaller amplitudes at lower redshift. More accurate formula for the bispectrum exists [39, 40] which can be incorporated in our analysis. Alternatively, the recently proposed separate Universe method can be employed to compute the higher-order integrated spectra [41–44]. In this approach the effect of long-wavelength density fluctuation on the small-scale power spectrum is computed by treating each over- and under dense region as a separate universe with a different background cosmology.

6.3 Integrated Bispectra in Lagrangian Perturbation Theory

The higher-order propagators take a particularly simpler form for the *Zeldovich Approimation* (ZA) (see e.g. Ref.[45] and references therein). The ZA is the first-order solution to perturbative dynamics formulated in Lagrangian space known as the Lagrangian Perturbation Theory (LPT) [8]. The second order kernel that describes the ZA is given by the following expression:

$$F_2^{\text{ZA}}(\mathbf{q}_1,\mathbf{q}_2) = \frac{1}{2}+\frac{1}{2}(\mathbf{q}_1\cdot\mathbf{q}_2)\left(\frac{1}{q_1^2}+\frac{1}{q_2^2}\right)+\frac{1}{2}\left(\frac{\mathbf{q}_1\cdot\mathbf{q}_2}{q_1\,q_2}\right)^2. \qquad (6.17)$$

This is a special case of the generic bispectrum studied in Eq.(6.1) for $\{\alpha,\beta\} = \{1/2, 1/2\}$. Using these expressions we can deduce the expression for the squeezed bispectrum in the leading order as:

$$\begin{aligned}& B_{\text{ZA}}(\mathbf{k}-\mathbf{q}_1,-\mathbf{k}+\mathbf{q}_{13},-\mathbf{q}_3) \\ & = \left[1+2\left(\frac{\mathbf{k}\cdot\mathbf{q}_3}{kq_3}\right)^2-\left(\frac{\mathbf{k}\cdot\mathbf{q}_3}{kq_3}\right)^2\frac{d\ln P(k)}{d\ln k}\right]P(k)P(q_3)+\mathcal{O}(q_3/k). \qquad (6.18)\end{aligned}$$

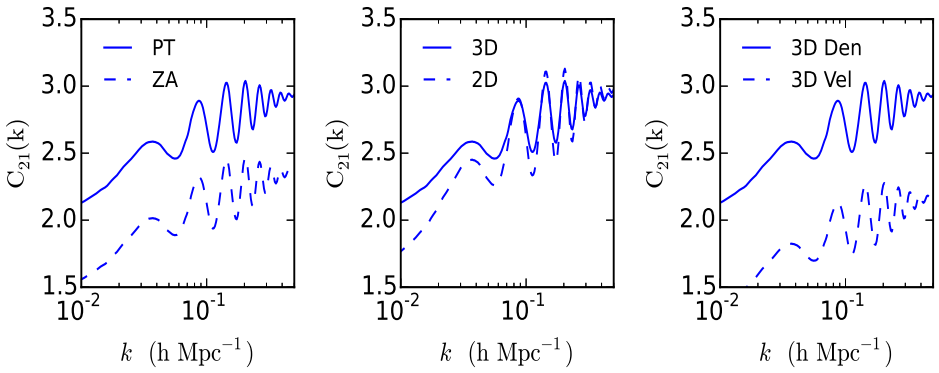

Figure 2: The left panel shows the integrated bispectrum from second-order Eulerian perturbation theory and the lowest order Lagrangian perturbation theory, the ZA, following Eq.(6.19). The middle panel compares the integrated bispectrum for 3D and 2D surveys Eq.(7.16). Finally, the right panel compares the integrated bispectrum for the density δ and the divergence of Θ.

The ZA and its higher-order analogues are often used to set-up the initial conditions in a numerical simulation [46]. The results can be derived using the same steps followed in the derivation of results from Eulerian perturbative dynamics Eq.(3.4) and Eq.(3.5). We quote the results here:

$$B_{\rm ZA} \overset{\rm squeeze}{\approx} \left[\frac{8}{3} - \frac{1}{3}\frac{d\ln k^3 P(k)}{d\ln k}\right] P(k)P(q_3) = \left[\frac{8}{3} - \frac{(n+3)}{3}\right] P(k)P(q_3). \tag{6.19}$$

Eq.(6.19) is a special case of the general result presented in Eq.(6.3) for $\{\alpha,\beta\} = \{1/2, 1/2\}$. These can be used to gauge the level of transients arising from the initial conditions often used in numerical simulations [46–48]. It is possible to compute the corrections from higher order LPT following the same procedure (see e.g. [45]). Squeezed configurations of the trispectrum can also be computed in a similar manner. The higher order kernels for the ZA are given in Eq.(A.7).

The integrated bispectrum for the ZA is presented in the left panel of Figure 2. The solid curve shows the prediction from second order SPT and the dashed line represents the ZA. For the entire range of k, the ZA under predicts the integrated bispectrum. This is related to the fact that the vertex $\nu_2 = 4/3$ for ZA as compared to $\nu_2 = 34/21$ for the exact dynamics. This values are consistent with skewness parameter $S_3 = 3\nu_2 = 34/7$ for SPT and $S_3 = 4$ for ZA [45]. For $n = -3$ we recover the limit $C_{21} = 2\nu_2 = 8/3$. Finally, using Eq.(5.9), the integrated bispectrum for the ZA takes the following form:

$$\bar{\mathcal{B}}_{ZA}(k) = \left[\frac{8}{3} - \frac{(n+3)}{3}\right] P(k)\sigma_L^2. \tag{6.20}$$

7 Integrated Bispectrum from Projected (2D) surveys

In this Section, we generalise the expression derived in 3D above to 2D or projected surveys. We consider 2D weak lensing surveys and 2D projected galaxy surveys. Though we eventually specialise the results to projected galaxy surveys, the results are equally relevant for studies of weak lensing and CMB secondaries (e.g. for the thermal Sunyaev Zeldovich (tSZ) effect). The results derived here can also generalised to *cross-correlation* of two different surveys or for *tomographic* analysis.

We start by defining an arbitrary projected field $\psi(\boldsymbol{\gamma})$ defined on the surface of the sky obtained through the line-of-sight integration of the 3D field $\Psi(r, \boldsymbol{\gamma})$:

$$\begin{aligned}\psi(\boldsymbol{\gamma}) &= \int_0^{r_s} dr\, w(r)\, \Psi(r, \boldsymbol{\gamma});\\ \psi(\boldsymbol{\gamma}) &= \int_0^{r_s} dr\, w(r) \int \frac{d^3k}{(2\pi)^3} \exp[i(\, r\, k_\parallel + d_A(r)\boldsymbol{\gamma}\cdot\mathbf{k}_\perp)]\Psi(\mathbf{k}).\end{aligned} \tag{7.1}$$

Here r is the comoving radial distance and $d_A(r)$ is the comoving angular diameter distance. ω is a generic radial selection function. $k_\parallel$ and $\mathbf{k}_\perp = d_A(r)\boldsymbol{\ell}$ are the radial and projected components of the wave-vector $\mathbf{k}$.

We will use small angle approximation (also known as the plane parallel approximation or the distant observer approximation). Generalisation to all-sky can be done in a straightforward manner using a speherical harmonic decomposition. The average of a projected field $\psi(\boldsymbol{\gamma})$ on the surface of the sky ($\boldsymbol{\gamma}$ here represents unit vector along a specific direction) is defined as:

$$\bar{\psi}(\boldsymbol{\gamma}_0) = \frac{1}{\Omega}\int d^2\boldsymbol{\gamma}\, \psi(\boldsymbol{\gamma}) W_{2\rm D}(\boldsymbol{\gamma}-\boldsymbol{\gamma}_0); \quad \Omega = \int d^2\boldsymbol{\gamma}\, W_{2\rm D}(\boldsymbol{\gamma}-\boldsymbol{\gamma}_0). \tag{7.2}$$

Here W_{2D} is the 2D mask that encodes the sky coverage and Ω is the area of the sky covered. The window function defined as $W_{2D}(\boldsymbol{\gamma}) \equiv \prod_{i=1}^{i=2}\theta(\boldsymbol{\gamma}_i)$. The one-dimensional unit step functions are the same as the ones defined in the 3D context in the previous section. Indeed, it is possible to generalise the results to arbitrary apodization using the pseudo-$\mathcal{C}_\ell$ approach [49]. The 2D Fourier transform assuming a flat sky takes the following form:

$$\psi(\boldsymbol{\ell}, \boldsymbol{\gamma}_0) = \int \frac{d^2\boldsymbol{\ell}'}{(2\pi)^2}\psi(\boldsymbol{\ell}-\boldsymbol{\ell}')\, W_{2\rm D}(\boldsymbol{\ell}')\, \exp(-i\boldsymbol{\gamma}_0\cdot\boldsymbol{\ell}'). \tag{7.3}$$

The *local* 2D power spectrum in this fraction of sky is given by:

$$\begin{aligned}P_{2\rm D}(\boldsymbol{\ell}, \boldsymbol{\gamma}_0) \equiv \frac{1}{\Omega}|\psi(\boldsymbol{\ell}, \boldsymbol{\gamma}_0)|^2 = \frac{1}{\Omega}\int \frac{d^2\boldsymbol{\ell}_1}{(2\pi)^2}\int \frac{d^2\boldsymbol{\ell}_2}{(2\pi)^2}\psi(\boldsymbol{\ell}-\boldsymbol{\ell}_1)\psi(-\boldsymbol{\ell}-\boldsymbol{\ell}_2)\\ \times \exp(-i\,\boldsymbol{\gamma}_0\cdot(\boldsymbol{\ell}_1+\boldsymbol{\ell}_2))W_{2\rm D}(\boldsymbol{\ell}_1)W_{2\rm D}(\boldsymbol{\ell}_2).\end{aligned} \tag{7.4}$$

The resulting integrated 2D bispectrum $\mathcal{B}_{2\rm D}$ is defined by cross-correlating the local estimate of the power spectrum and the local average of the projected field.

$$\mathcal{B}_{2\rm D}(\boldsymbol{\ell}) \equiv \langle P_{2\rm D}(\boldsymbol{\ell}, \boldsymbol{\gamma}_0)\bar{\psi}(\boldsymbol{\gamma}_0)\rangle_c; \tag{7.5}$$

$$\begin{aligned}\mathcal{B}_{2\rm D}(\boldsymbol{\ell}) = \frac{1}{\Omega^2}\int \frac{d^2\boldsymbol{\gamma}}{4\pi}\int \frac{d^2\boldsymbol{\ell}_1}{(2\pi)^2}\int \frac{d^2\boldsymbol{\ell}_2}{(2\pi)^2}\int \frac{d^2\boldsymbol{\ell}_3}{(2\pi)^2}\langle\psi(\boldsymbol{\ell}-\boldsymbol{\ell}_1)\psi(-\boldsymbol{\ell}-\boldsymbol{\ell}_2)\psi(-\boldsymbol{\ell}_3)\rangle\\ \times W_{2\rm D}(\boldsymbol{\ell}_1)W_{2\rm D}(\boldsymbol{\ell}_2)W_{2\rm D}(\boldsymbol{\ell}_3)\exp(-i\,\boldsymbol{\gamma}_0\cdot(\boldsymbol{\ell}_1+\boldsymbol{\ell}_2+\boldsymbol{\ell}_3)).\end{aligned} \tag{7.6}$$

We have used the following relations along with Eq.(7.3):

$$\psi(\boldsymbol{\ell},\boldsymbol{\gamma}_0) = \int d^2\boldsymbol{\gamma}\ \ \psi(\boldsymbol{\gamma})W_{\rm 2D}(\boldsymbol{\gamma}-\boldsymbol{\gamma}_0)\exp(i\boldsymbol{\ell}\cdot\boldsymbol{\gamma}); \quad \bar{\psi}(\boldsymbol{\gamma}_0) = \frac{1}{\Omega}\psi(\mathbf{0},\boldsymbol{\gamma}_0). \tag{7.7}$$

[[Here $\psi(\boldsymbol{\ell},\gamma_0)$ is local Fourier transform and $\bar{\psi}$ is the mean projected density.
The projected power spectrum $P_{\rm 2D}(\boldsymbol{\ell})$ and bispectrum $B_{\rm 2D}(\boldsymbol{\ell}_1,\boldsymbol{\ell}_2,\boldsymbol{\ell}_3)$:]]

$$\langle\psi(\boldsymbol{\ell}_1)\psi(\boldsymbol{\ell}_2)\rangle_c \equiv (2\pi)^2\delta_{\rm 2D}(\boldsymbol{\ell}_{12})P_{\rm 2D}(\boldsymbol{\ell}_1); \tag{7.8}$$

$$\langle\psi(\boldsymbol{\ell}_1)\psi(\boldsymbol{\ell}_2)\psi(\boldsymbol{\ell}_3)\rangle_c \equiv (2\pi)^2\delta_{\rm 2D}(\boldsymbol{\ell}_{123})B_{\rm 2D}(\boldsymbol{\ell}_1,\boldsymbol{\ell}_2,\boldsymbol{\ell}_3). \tag{7.9}$$

They can be expressed in terms of their 3D counterparts through line-of-sight integrations:

$$P_{\rm 2D}(\ell) \equiv \int_0^{r_s} d\,r\frac{\omega^2(r)}{d_A^4(r)}P_{3D}\left(\frac{\ell}{d_A(r)}\right); \tag{7.10}$$

$$B_{\rm 2D}(\boldsymbol{\ell}_1,\boldsymbol{\ell}_2,\boldsymbol{\ell}_3) \equiv \int_0^{r_s} d\,r\frac{\omega^3(r)}{d_A^6(r)}B_{\rm 3D}\left(\frac{\boldsymbol{\ell}_1}{d_A(r)},\frac{\boldsymbol{\ell}_2}{d_A(r)},\frac{\boldsymbol{\ell}_3}{d_A(r)}\right)_{\sum\boldsymbol{\ell}_i=0}; \tag{7.11}$$

see Ref.[50] and reference therein. The expression for $B_{\rm 3D}$ is given in Eq.(A.17). The angular average of the integrated bispectrum in 2D $\bar{\mathcal{B}}_{\rm 2D}(\ell)$, can be defined as follows:

$$\bar{\mathcal{B}}_{\rm 2D}(\ell) = \int\frac{d\theta_\ell}{2\pi}\,\mathcal{B}_{\rm 2D}(\boldsymbol{\ell}); \quad \ell = |\boldsymbol{\ell}|. \tag{7.12}$$

The complete expression for the angular averaged integrated bispectrum $\bar{\mathcal{B}}_{\rm 2D}(\boldsymbol{\ell})$ takes the following form:

$$\begin{aligned}\bar{\mathcal{B}}_{\rm 2D}(\boldsymbol{\ell}) \equiv \int\frac{d\theta_\ell}{2\pi}\int\frac{d^2\boldsymbol{\ell}_1}{(2\pi)^2}\int\frac{d^2\boldsymbol{\ell}_3}{(2\pi)^2}B_{\rm 2D}(\boldsymbol{\ell}-\boldsymbol{\ell}_1,-\boldsymbol{\ell}+\boldsymbol{\ell}_1+\boldsymbol{\ell}_3,-\boldsymbol{\ell}_3)\\ \times\ W_{\rm 2D}(\boldsymbol{\ell}_1)W_{\rm 2D}(-\boldsymbol{\ell}_1-\boldsymbol{\ell}_3)W_{\rm 2D}(\boldsymbol{\ell}_3).\end{aligned} \tag{7.13}$$

We have used the Dirac delta function in Eq.(7.9) to collapse the $\boldsymbol{\ell}_2$ integral. In the *squeezed limit* the 2D bispectrum $B_{\rm 2D}($ takes following form:

$$\begin{aligned}&B_{\rm 2D}(\boldsymbol{\ell}-\boldsymbol{\ell}_1,-\boldsymbol{\ell}+\boldsymbol{\ell}_1+\boldsymbol{\ell}_3,-\boldsymbol{\ell}_3)\\ &= \left[\frac{13}{7}+\frac{8}{7}\left(\frac{\boldsymbol{\ell}\cdot\boldsymbol{\ell}_3}{\ell\ell_3}\right)^2-\left(\frac{\boldsymbol{\ell}\cdot\boldsymbol{\ell}_3}{\ell\ell_3}\right)^2\frac{d\ln P_{\rm 2D}(\ell)}{d\ln\boldsymbol{\ell}}\right]P(\boldsymbol{\ell})P(\boldsymbol{\ell}_3)+\cdots\end{aligned} \tag{7.14}$$

The terms of higher order in (ℓ_1/ℓ) or (ℓ_3/ℓ) are ignored as we take the limiting case when $\ell \gg \ell_i$. Using the fact that the circular average of $\hat{\boldsymbol{\ell}}\cdot\hat{\boldsymbol{\ell}}_3$ is [1/2] we arrive at the following expression:

$$\bar{\mathcal{B}}_{\rm 2D}(\ell) = K_3\left[\frac{24}{7}-\frac{1}{2}\frac{d\ln\ell^2P(\ell)}{d\ln\ell}\right]P_{\rm 2D}(\ell)\sigma^2(\theta_0); \tag{7.15}$$

$$K_3 = \int_0^{r_s}dr\frac{w^3(r)}{d_A^{(6+2n)}(r)}\Big/\left[\int_0^{r_s}dr\frac{w^2(r)}{d_A^{(4+n)}(r)}\right]^2. \tag{7.16}$$

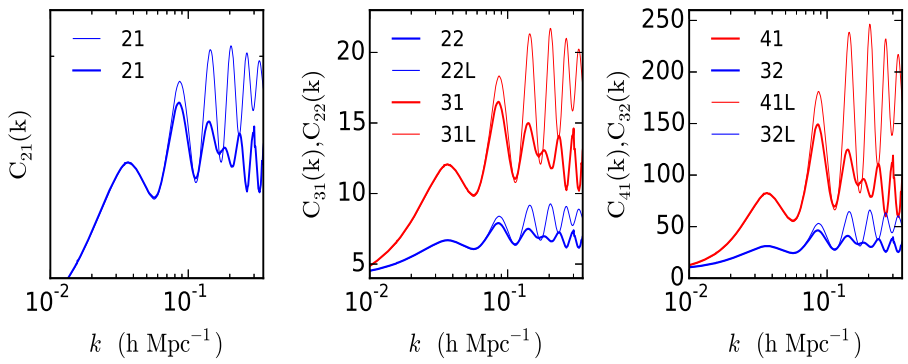

Figure 3: The 3D normalised cumulant corelators [defined in Eq.(3.4)-Eq.(3.5)] are plotted. The plots show $C_{21}(k)$ (left panel), $C_{31}(k)$ and $C_{22}(k)$ (middle panel) and $C_{41}(k)$ and $C_{32}(k)$ (right panel) as a function of the k wave number. The results are derived using a standard perturbation theory (SPT) and power spectrum including one-loop corrections. The results shown are for z=0 (see text for more details).

This matches the published results on cumulant correlators quoted below in Eq.(7.17) for a 3D power spectrum which can be described locally as a power-law with a slope n i.e. $P(k) \propto k^n$. The corresponding cumulant correlators are derived in [51]:

$$C_{21}^{2D} = \frac{24}{7} - \frac{1}{2}(n+2); \tag{7.17}$$

$$C_{31}^{2D} = \frac{1473}{49} - \frac{195}{14}(n+2) + \frac{3}{2}(n+2)^2. \tag{7.18}$$

Using very similar arguments we can show that if we assume a HA for the underlying 3D bispectrum Eq.(4.13), the corresponding integrated bispectrum is given by:

$$\bar{\mathcal{B}}_{2D}(\ell) = 2K_3\, Q_3\, P_{2D}(\ell)\sigma^2_{2D}(\theta_0); \quad \sigma^2_{2D}(\theta_0) \equiv \int \frac{d\ell}{4\pi}\ell P(\ell) W^2_{2D}(\ell\theta_0). \tag{7.19}$$

The integrated bispectrum $\bar{\mathcal{B}}_{2D}(\ell)$ in 2D is plotted in Figure 3 as a function of ℓ (middle panel). The expression for the multiplicative factor K_3 in Eq.(7.19) depends on the survey geometry and selection function which is not included in the plot.

These results can readily be extended to the case of two different surveys with overlapping sky coverage but different radial selection functions or for surveys with tomographic bins.

8 Results and Discussion

The position-dependent power spectrum, a probe of squeezed configuration of bispectrum, was recently proposed as a method to probe galaxy clustering. Cumulant correlators and their Fourier transform, the skew-spectra, are also often used to probe the primary or secondary

non-Gaussianity. In this paper, we have compared these two techniques and elucidated their relationship to one another.

First, we have generalised the concept of skew-spectrum and kurt-spectrum defined at third and fourth-order to arbitrary order. We used known perturbative results to show [Eq.(2.10)] in the large separation limit, or low $\mathbf{k}$ limit ($\mathbf{k} \to 0$), the generalisations of skew-spectra defined in Eq.(2.4) to higher-order, also known as the multispectra $S_{pq}(k)$, are proportional to the underlying power spectrum with proportionality constants C_{pq} [see e.g. Eq.(3.4)] that are known to arbitrary order. The proportionality constants depend on the local (linear) power-spectral index n at the smoothing scale and can be computed to arbitrary order. These coefficients, deduced using a top-hat smoothing window, are known in 2D and 3D, and are related to two-point joint PDFs $p_\delta(\delta_1, \delta_2)$ or equivalently the bias $b(\delta)$, defined in Eq.(3.9), of overdense objects. The computation of $S_{pq}(k)$ for the entire range of k requires numerical evaluation. This has been carried out in for the $S_{21}(k)$ in Ref.[53] for 3D galaxy surveys. Notice that the skew-spectra and kurt-spectra have also been employed in analysing primordial non-Gaussianity in CMB temperature maps (Ref.[5, 6]). However the mulrispectra that we consider here are sub-optimal, where as, for CMB studies *optimised* versions were considered to improve their sensitivity to primordial non-Gaussianity. Indeed inverse variance weighting of the data vector can be introduced in their construction in which case these estimators will be identical to squeezed limit of the skew-spectra statistics developed in Ref.[5].

Next, we generalised the concept of a position-dependent power spectrum or integrated bispectrum (IB) of the density field δ in many directions. We use a unifying approach in §6 to investigate IB. Using a generic bispectrum Eq.(6.1) we have deduced the IB for δ and Θ in Eq.(6.9) from a master Eq.(6.3) that can also deal, with the bispectrum from lowest order of Lagrangian perturbation theory, the ZA. Using Limber's approximation, we have also applied this result to projected (2D) surveys in §7. These results can be readily generalised to tomographic surveys or to cross-correlation of overlapping surveys using two different tracer fields. Extending the concept of IB for one field we have generalised it to consider (δ-Θ) mixed bispectrum in §6.2. In Eq.(6.12)-Eq.(6.16) we have pointed out that such measurements are sensitive to cosmological parameter Ω. The results for ZA will particularly be useful in assessing magnitude of transients in numerical simulation. Using the unifying approach, we were able to show that in each of these specific cases the expressions for $\mathrm{C}_{21}(k)$ and $\bar{\mathcal{B}}(k)$ share the same analytical expression Eq.(6.8). Despite the formal mathematical similarities, the actual interpretation is quite different. In case of cumulant correlator C_{21} a given smoothing scale R_0 dictates the spectral index n. To map out the entire range of k a range of smoothing scales are needed. Similarly, the momentum or k-dependence of the integrated bispectrum $\bar{\mathcal{B}}(k)$ can only be probed using many sub-samples of the survey and taking an ensemble average. Each sub-sample probes the entire allowed k range but only provides a noisy estimate. Both methods can be used simultaneously as a consistency check. The power law $n = -3$ correspond to the case of no smoothing. In this case we recover the scale independent HA value of $2\bar{Q} \equiv 2\nu_2 = 68/21$ using the angular average of Q i.e. $\bar{Q} = 34/21$ [see eq.(4.17)]. Notice that this is true also for 2D and divergence of velocity Θ. In the case of Θ, the unsmoothed vertex takes the numerical value: $Q_3 = 2\bar{G} = 52/21$.

Going beyond second-order in Standard (Eulerian) Perturbation Theory (SPT) we have extended the concept of IB to integrated trispectrum (IT) in Appendix-§A. We introduced two ITs at the level of trispectrum: $\mathcal{B}_{22}(k)$ and $\mathcal{B}_{31}(k)$ respectively in Appendix-§B and Appendix§C. In the *soft* limit they correspond to squeezed and collapsed limits of the trispec-

trum. They are analogues of the corresponding cumulant correlators $\mathrm{C}_{22} = \mathrm{C}_{21}^2$ and C_{31} respectively. The IT $\mathcal{B}_{22}(k)$ can be constructed using the expression for the $\mathcal{B}_{21}(k)$ [Eq.(B.12)] and shows a structural similarity with C_{22}. The explicit evaluation of $\mathcal{B}_{31}(k)$ was recently performed in Ref.[54]. However, the functional form for $\mathcal{B}_{31}(k)$ [Eq.(C.24)-Eq.(C.25)] is not same as that of $\mathrm{C}_{31}(k)$. We expect the same to be true for higher order integrated spectra. However, extension of these results to higher orders can be cumbersome owing to the complicated structure of the higher-order kernels F_n see Eq.(A.3). We conclude that higher-order multispectra and higher-order integrated spectra can provide complementary information and much needed consistency checks on probes of non-Gaussianity in diverse cosmological data sets.

In addition to the SPT and LPT we have used the HA to get insight into soft limits of higher order polyspectra [Eq.(4.1)-Eq.(4.4)]. In HA the tree perturbative hierarchy is replaced with a similar hierarchy, but where the kernels F_n and G_n are replaced by vertices ν_n and μ_n which are angular averages of these kernels [Eq.(A.8)-Eq.(A.9)]. Many different models of HA exist and it is indeed possible also to leave these vertices as unknown parameters. This model is only valid in the highly non-linear regime and thus strictly speaking not suitable for taking $\mathbf{k} \to 0$. However, it provides very useful insight in higher order where exact SPT results are prohibitively complicated especially in an idealised situation of $n = -3$ when smoothing can be ignored. The squeezed limit for the HA bispectrum is given in Eq.(4.16) and the collapsed and squeezed limits of the trispectrum are presented in Eq.(4.18) and Eq.(4.19) respectively.

The CCs and higher order integrated spectra both depend only on one wave number so they are much easier to estimate than the corresponding full polyspectra. It is also much simpler to compute their covariance.

In this paper we have primarily focused on the theoretical aspects of IB and IT. We have shown that with other related statistics CCs and integrated spectra can play complementary rule in probing soft limits of higher order polyspectra in 3D or projection (2D).

However, to use the estimators proposed here it will be important to develop them further. For example it's important to include redshift space distortion to analyse galaxy surveys - which will involve analysing soft limits of polyspectra in redshift space [55]. Our results here are based on perturbative analysis, but, including results from halo model can be done in a relatively straightforward manner to extend the range of validity. Similarly, it is not difficult to extend the results here to include primordial non-Gaussianity, though they remain highly constrained by recent CMB observations [56] at least at scales probed by CMB observations.

For weak lensing surveys, going beyond the 2D or tomographic analysis presented here it is now becoming practical to analyse the data in 3D. Weak lensing probes structure formation at small scale. Gravity induced non-Gaussianity is known to provide additional information to constrain the cosmology. Our approach developed here can be generalised to 3D weak lensing surveys using a spherical Fourier-Bessel transformation [57, 58]. In the field of CMB research, squeezed configuration of primordial non-Gaussianity and its effect on CMB lensing have been investigated [59, 60]. Two important secondaries - the lensing of CMB [61], and the kSZ effect - both have a vanishing bispectrum [62]. They do not have any frequency information either. Thus the two sets of IT discussed here can be useful in separating these two secondaries. Results presented here will also be useful in analysing frequency-cleaned y-parameter maps [63] or to study squeezed limit of bispectrum induced by reionization [64]. These estimators can also generalised to cross-correlate weak-lensing κ maps and y maps [65]. The *separate universe* approach developed by several authors remain a possibility for such

development [41–44]. Indeed the morphological estimators or the Minkowski Functionals (MF) are a popular method to study non-Gaussianity in cosmological fields. MFs depend on the higher order polyspectra and squeezed limit of polyspectra can also be related to the position dependent MFs. The study of soft limit of polyspectra for CMB secondaries may provide a method to test the kinematic consistency relations to constrain modified gravity theories or primordial non-Gaussianity [66].

Estimation of integrated spectra (IB or IT) is undoubtedly simpler than the corresponding polyspectra, but designing optimal estimators to extract information about higher-order non-Gaussianities it is not a simple task. A particular difficulty is posed by the need to estimate the sample variance arising from the survey. The scatter in the IB we deduced in this paper used a very simple prescription that ignores the very non-Gaussianity we seek to characterise. In a regime in which the approximation of mild non-Gaussianity breaks down such a treatment will become inadequate.

Finally, note that the estimators developed here are sub-optimal. Though may not be too serious a concern for high quality data sets but in any case they are valuable by virtue of being much easier to implement in practice than optimal estimators.

9 Acknowledgements

DM and PC acknowledge support from the Science and Technology Facilities Council (grant number ST/L000652/1).

References

[1] SDSS-III: Massive Spectroscopic Surveys of the Distant Universe, the Milky Way Galaxy, and Extra-Solar Planetary Systems Eisenstein, D. J., Weinberg, D. H., Agol, E., et al. 2011, AJ, 142, 72, [arXiv:1101.1529]

[2] The WiggleZ Dark Energy Survey: Survey Design and First Data Release, Drinkwater, M. J., Jurek, R. J., Blake, C., et al. 2010, MNRAS, 401, 14, [arXiv:0911.4246]

[3] The Dark Energy Survey, The Dark Energy Survey Collaboration 2005, arXiv:astro-ph/0510346, [astro-ph/0510346].

[4] Euclid Definition Study Report Laureijs, R., Amiaux, J., Arduini, S., et al. 2011, arXiv:1110.3193, [arXiv:1110.3193].

[5] A New Approach to Probing Primordial Non-Gaussianity, Munshi D., Heavens A., 2010, MNRAS, 401, 2406, [arXiv/0904.4478].

[6] New Optimised Estimators for the Primordial Trispectrum, Munshi D., Heavens A., Cooray A., Smidt J., Coles P., Serra P., 2011, MNRAS, 412,1993, [arxiv/0910.3693].

[7] From Weak Lensing to non-Gaussianity via Minkowski Functionals Munshi D., van Waerbeke L., Smidt J., Coles P., 2012, MNRAS, 419, 536

[8] Large scale structure of the universe and cosmological perturbation theory, Bernardeau F., Colombi S., Gaztanaga E., Scoccimarro R., 2002, Phys.Rept. 367, 1, [astro-ph/0112551].

[9] The Effective Field Theory of Cosmological Large Scale Structures Joseph J., Carrasco M., Hertzberg M.P., Senatore L. JHEP, Volume 2012, Number 9 (2012), 82, [arXiv:1206.2926]

[10] Halo Models of Large Scale Structure Cooray A., Sheth R. 2002, Phys.Rept.372, 1, [astro-ph/0206508]

[11] Position-dependent power spectrum of the large-scale structure: a novel method to measure the squeezed-limit bispectrum, Chiang C-T, Wagner C.,Schmidt F., Komatsu E., [arXiv/1403.3411].

[12] The large-scale Gravitational Bias from the Quasilinear Regime, Bernardeau F., 1996, A&A 312, 11 [arXiv/9602072].

[13] Generalised Cumulant Correlators and Hierarchical Clustering, Munshi D.; Melott A. L., Coles P., 2000, MNRAS, 311, 149 [arXiv/9812271].

[14] The Separate Universe Approach to Soft Limits, Kenton Z., Mulryne D.J., [arXiv/1605.03435]

[15] Kinematic consistency relations of large-scale structures, Valageas P., 2014, PRD, 89, 083534 [arXiv/1311.1236]

[16] Angular averaged consistency relations of large-scale structures, Valageas P., 2014, PRD, 89, 123522, [arXiv/1311.4286]

[17] Testing the equal-time angular-averaged consistency relation of the gravitational dynamics in N-body simulations Nishimichi T., Valageas P., 2014, PRD, 90, 023546, [arXiv/1402.3293]

[18] Hyperextended Cosmological Perturbation Theory: Predicting Non-linear Clustering Amplitudes, Scoccimarro R., Frieman J.A., 1999, ApJ, 520, 35 [astro-ph/9811184].

[19] Cumulant Correlators from the APM, Szapudi I., Szalay A.S., 1999, Astrophys.J., 515, L43, [astro-ph/9702015].

[20] Weak lensing from strong clustering, Munshi, D; Coles, P, 2000, MNRAS, 313, 148, [astro-ph/9911008].

[21] On the integration of the BBGKY equations for the development of strongly nonlinear clustering in an expanding universe, Davis M., Peebles, P.J.E. 1977, ApJS, 34, 425, [1977 ApJS 34 425D]

[22] Statistical Analysis Of Catalogs Of Extragalactic Objects. VII -Two- And -Three- Point Correlation Functions For The High-Resolution Shane-Wirtanen Catalog Of Galaxies, Groth E., Peebles, P.J.E., 1977, ApJ, 217, 385, [1977 ApJ 217 385G]

[23] The Galaxy correlation hierarchy in perturbation theory Fry J.N., 1984b, ApJ, 279, 499, [1984 ApJ 279 499F]

[24] The gravity-induced quasi-Gaussian correlation hierarchy Bernardeau, F. 1992, ApJ, 192, 1, [1992 ApJ 392 1B]

[25] The Effects of Smoothing on the Statistical Properties of the Large-Scale Cosmic Fileds Bernardeau, F. 1994, A&A, 291, 697, [astro-ph/9403020].

[26] Statistical analysis of catalogs of extragalactic objects. IX - The four-point galaxy correlation function Fry J.N., Peebles P.J.E., 1978, ApJ, 221, 19, [1978 ApJ 221 19F]

[27] Peebles, P.J.E. 1980, The Large Scale Structure of the Universe, Princeton University Press, Princeton, N.J., USA

[28] Scale-invariant matter distribution in the universe. I - Counts in cells, Balian R., Schaeffer R., 1989, A&A, 220, 1

[29] Hamilton, A.J.S., 1988b, ApJ, 332, 67

[30] Reconstructing the primordial spectrum of fluctuations of the universe from the observed nonlinear clustering of galaxies. Hamilton, A.J.S., Kumar, P., Lu, E., Mattews, A. 1991, ApJ, 274, 1; Erratum: 1995, ApJ, 442L, 73H, [1991 ApJ 374L 1H]

[31] Halo correlations in nonlinear cosmic density fields. Bernardeau F., Schaeffer R., 1999, A&A, 349, 697B, [astro-ph/990387].

[32] Galaxy correlations, matter correlations and biasing, Bernardeau F., Schaeffer R., 1992, A&A, 255, 1

[33] Bias and Hierarchical Clustering, Coles P., Melott A.L., Munshi D., 1999, ApJ, 521L, 5C,

[astro-ph/9904253]

[34] From Snakes to Stars, the Statistics of Collapsed Objects - I. Lower-order Clustering Properties, Munshi D., Coles P., Melott A.L. 1999, MNRAS, 307, 387, [astro-ph/9812337]

[35] From Snakes to Stars, the Statistics of Collapsed Objects - II. Lower-order Clustering Properties, Munshi D., Coles P., Melott A.L., 1999, MNRAS, 310, 892, [astro-ph/9902215]

[36] Scaling in Gravitational Clustering, 2D and 3D Dynamics, Munshi D., Bernardeau F., Melott A.L., Schaeffer R., 1999, MNRAS, 303, 433, [astro-ph/9707009]

[37] The Effect of a Lumpy Matter Distribution on the Growth of Irregularities in an Expanding Universe, P. J. E. Peebles, 1974, A&A, 32, 391.

[38] Omega from the skewness of the cosmic velocity divergence, Bernardeau F., Juszkiewicz R., Dekel A., Bouchet F.R., 1995, MNRAS, 274, 20, [astro-ph/9404052].

[39] Scoccimarro R., Couchman, H.M. 2011, MNRAS, 325, 1312, [astro-ph/009427]

[40] An improved fitting formula for the dark matter bispectrum Gil-Marn H., Wagner C., Fragkoudi F., Jimenez R., Verde L., 2012, JCAP, 02, 047 [astro-ph/111.4477]

[41] Galaxy Bias and non-Linear Structure Formation in General Relativity, T. Baldauf, U. Seljak, L. Senatore, and M. Zaldarriaga, 2011, JCAP, 1110, 031 [arXiv/1106.5507].

[42] Single-Field Consistency Relations of Large Scale Structure Creminelli P, Norea J., Simonovi M., Vernizzi F. 2013, JCAP, 12, 025C [arxiv/1309.3557]

[43] Super-Sample Covariance in Simulations Li Y., Hu W., Takada M., 2014, PRD, 89, 083519 [arxiv/1401.0385]

[44] The Observed squeezed limit of cosmological three-point functions, E. Pajer, F. Schmidt, and M. Zaldarriaga, 2013, PRD, 88, 083502, [arXiv/1305.0824].

[45] Munshi, D., Sahni, V., Starobinsky, A. A., Nonlinear approximations to gravitational instability: A comparison in the quasi-linear regime, 1994, ApJ, 436, 517M [astro-ph/9402065].

[46] Transients from Initial Conditions: A Perturbative Analysis Scoccimarro R., 2998, MNRAS, 299, 1097 [astro-ph/9711187]

[47] Transients from Initial Conditions in Cosmological Simulations M. Crocce, S. Pueblas, R. Scoccimarro 2006, MNRAS, 373, 369 [astro-ph/0606505]

[48] Transients from Zel'dovich initial conditions P. Valageas 2002, A&A, 385, 761 [astro-ph/0112102]

[49] MASTER of the CMB Anisotropy Power Spectrum: A Fast Method for Statistical Analysis of Large and Complex CMB Data Sets 2002, ApJ, 567, 2 [astro-ph/0105302]

[50] Cosmological parameters from lensing power spectrum and bispectrum tomography Takada M, Jain B., 2004, MNRAS, 348, 897 [arxiv/0310125]

[51] Weak Lensing Statistics as a Probe of Omega and Power Spectrum, F. Bernardeau, L. van Waerbeke, Y. Mellier, 1997, A&A. 322, 1, [astro-ph/9609122].

[52] The angular correlation hierarchy in the quasilinear regime, Bernardeau F., 1995, A&A, 301, 309 [arXiv/9502089].

[53] Non-Gaussianity in large-scale structure and Minkowski functionals Pratten G., Munshi D., 2012, MNRAS, 423, 3209, [arxiv/1108.1985]

[54] The angle-averaged squeezed limit of nonlinear matter N-point functions Wagner C, Schmidt F., Chiang C.-T., Komatsu E., 2015, JCAP, 08, 042, [arxiv/1503.03487]

[55] Galaxy clustering in 3D and modified gravity theories, Munshi D., Pratten G., Valageas P., Coles P., Brax Ph., 2016, MNRAS, 456, 1627 [arxiv/1508.00583]

[56] Planck 2015 results. XVII. Constraints on primordial non-Gaussianity Planck Collaboration [arxiv/1502.01592]

[57] 3D Weak Lensing: Modified Theories of Gravity Pratten G., Munshi D., Valageas P., Brax Ph., 2016, PRD, 93, 103524, [arxiv/1602.06711]

[58] Higher order statistics for three-dimensional shear and flexion Munshi D., Kitching T., Heavens A., Coles P., 2011, MNRAS, 416, 1629, [arxiv/1012.3658]

[59] CMB lensing and primordial squeezed non-Gaussianity, Pearson R., Lewis A., Regan D., 2012, JCAP, 03, 011, [arXiv:1201.1010]

[60] The full squeezed CMB bispectrum from inflation, Lewis A., 2012, JCAP, 06, 023, [arXiv:1204.5018]

[61] Lensing-induced morphology changes in CMB temperature maps in modified gravity theories, Munshi D., Hu B., Matsubara T., Coles P., Heavens A., 2016, JCAP, 04, 056 [arxiv/1602.00965]

[62] Extracting the late-time kinetic Sunyaev-Zel'dovich effect, D. Munshi, I. T. Iliev, K. L. Dixon, P. Coles [arxiv/1511.034495]

[63] Cross-correlating Sunyaev-Zel'dovich and weak lensing maps, Munshi D., Joudaki S., Coles P., Smidt J., Kay S. T., 2014, MNRAS, 442, 69 [arxiv/1111.5010]

[64] Reionization and CMB non-Gaussianity Munshi D., Corasaniti P. S., Coles P., Heavens A., Pandolfi S. [arXiv/1403.1531]

[65] Statistical Properties of Thermal Sunyaev-Zel'dovich Maps, Munshi D., Joudaki S., Smidt J., Coles P., Kay S. T., 2013, MNRAS, 429, 1564 [arxiv/1106.0706]

[66] Redshift-space equal-time angular-averaged consistency relations of the gravitational dynamics, Nishimichi T., Valageas P., 2015, PhRvD,92, 123510, [arxiv/1503.06036]

A Perturbation Theory: A Very Brief Review

We will briefly quote some results from Standard (Eulerian) Perturbation Theory (SPT) that are relevant in our context; more details can be found in Ref.[8]. The perturbative expansions of the density field δ and Θ can be expressed in terms of kernels F_n and G_n:

$$\begin{aligned}
&\delta(\mathbf{k}) = \delta^{(1)}(\mathbf{k}) + \delta^{(2)}(\mathbf{k}) + \cdots ; \\
&\delta^{(n)}(\mathbf{k}) = \int d^3\mathbf{q}_1 \cdots \int d^3\mathbf{q}_n F_n(\mathbf{q}_1, \cdots, \mathbf{q}_n)\delta(\mathbf{q}_1)\cdots\delta(\mathbf{q}_n). \qquad \text{(A.1)} \\
&\Theta(\mathbf{k}) = \Theta^{(1)}(\mathbf{k}) + \Theta^{(2)}(\mathbf{k}) + \cdots ; \\
&\Theta^{(n)}(\mathbf{k}) = \int d^3\mathbf{q}_1 \cdots \int d^3\mathbf{q}_n G_n(\mathbf{q}_1, \cdots, \mathbf{q}_n)\delta(\mathbf{q}_1)\cdots\delta(\mathbf{q}_n). \qquad \text{(A.2)}
\end{aligned}$$

The expressions for the nth order kernels F_n and G_n for δ and Θ respectively are Ref.[8]:

$$\begin{aligned}
F_n(\mathbf{q}_1, \cdots, \mathbf{q}_n) = \sum_{m=1}^{n-1} \frac{G_m(\mathbf{q}_1, \cdots, \mathbf{q}_m)}{(2n+3)(n-1)} [(2n+1)\alpha(\mathbf{k}_1, \mathbf{k}_2) F_{n-m}(\mathbf{q}_{m+1}, \cdots, \mathbf{q}_n) \\
+2\beta(\mathbf{k}_1, \mathbf{k}_2) G_{n-m}(\mathbf{q}_{m+1}, \cdots, \mathbf{q}_n)]. \qquad \text{(A.3)}
\end{aligned}$$

$$\begin{aligned}
G_n(\mathbf{q}_1, \cdots, \mathbf{q}_n) = \sum_{m=1}^{n-1} \frac{G_m(\mathbf{q}_1, \cdots, \mathbf{q}_m)}{(2n+3)(n-1)} [3\alpha(\mathbf{k}_1, \mathbf{k}_2) F_{n-m}(\mathbf{q}_{m+1}, \cdots, \mathbf{q}_n) \\
+2n\beta(\mathbf{k}_1, \mathbf{k}_2) G_{n-m}(\mathbf{q}_{m+1}, \cdots, \mathbf{q}_n)]. \qquad \text{(A.4)}
\end{aligned}$$

Here $F_1 = 1$ and $G_1 = 1$ and the functions α and β are defined as:

$$\alpha(\mathbf{k}_1, \mathbf{k}_2) \equiv \frac{\mathbf{k}_{12} \cdot \mathbf{k}_1}{k_1^2}; \quad \beta(\mathbf{k}_1, \mathbf{k_2}) \equiv k_{12}^2 \frac{\mathbf{k}_1 \cdot \mathbf{k}_2}{2k_1^2 k_2^2}. \tag{A.5}$$

We have defined the following quantities above:

$$\mathbf{k}_1 = \mathbf{q}_1 + \cdots + \mathbf{q}_m; \quad \mathbf{k}_2 = \mathbf{q}_{m+1} + \cdots + \mathbf{q}_n; \quad \mathbf{k} = \mathbf{k}_1 + \mathbf{k}_2. \tag{A.6}$$

The vertices $F_n^{\rm ZA}$ for the lowest order Lagrangian Perturbation Theory (LPT) or ZA take the following form:

$$F_n^{\rm ZA}(\mathbf{q}_1, \cdots, \mathbf{q}_n) = \frac{1}{n!} \frac{\mathbf{k} \cdot \mathbf{q}_1}{q_1^2} \cdots \frac{\mathbf{k} \cdot \mathbf{q}_n}{q_n^2}; \qquad \mathbf{k} \equiv \mathbf{q}_1 + \cdots + \mathbf{q}_n. \tag{A.7}$$

The angular averages of the kernels are the tree-levels amplitudes or the vertices as defined below:

$$\nu_n \equiv n! \int \frac{d\hat{\Omega}_1}{4\pi} \cdots \int \frac{d\hat{\Omega}_n}{4\pi} F_n(\mathbf{k}_1, \cdots \mathbf{k}_n); \tag{A.8}$$

$$\mu_n \equiv n! \int \frac{d\hat{\Omega}_1}{4\pi} \cdots \int \frac{d\hat{\Omega}_n}{4\pi} G_n(\mathbf{k}_1, \cdots \mathbf{k}_n). \tag{A.9}$$

Using Eq.(A.3) and Eq.(A.4) the second and third order kernels are defined as follows:

$$F_2(\mathbf{k}_1, \mathbf{k}_2) \equiv \frac{5}{7} + \frac{1}{2}\left(\frac{1}{k_1^2} + \frac{1}{k_2^2}\right)(\mathbf{k}_1 \cdot \mathbf{k}_2) + \frac{2}{7}\frac{(\mathbf{k}_1 \cdot \mathbf{k}_2)^2}{k_1^2 k_2^2}; \tag{A.10}$$

$$\begin{aligned} F_3(\mathbf{k}_1, \mathbf{k}_2, \mathbf{k}_3) = {} & \frac{7}{18}\frac{\mathbf{k}_{12} \cdot \mathbf{k}_1}{k_1^2}\left[F_2(\mathbf{k}_2, \mathbf{k}_3) + G_2(\mathbf{k}_1, \mathbf{k}_2)\right] \\ & + \frac{2}{18}\frac{\mathbf{k}_{12}^2(\mathbf{k}_1 \cdot \mathbf{k}_2)}{k_1^2 k_2^2}\left[G_2(\mathbf{k}_2, \mathbf{k}_3) + G_2(\mathbf{k}_1, \mathbf{k}_2)\right]. \end{aligned} \tag{A.11}$$

$$G_2(\mathbf{k}_1, \mathbf{k}_2) \equiv \frac{3}{7} + \frac{1}{2}\left(\frac{1}{k_1^2} + \frac{1}{k_2^2}\right)(\mathbf{k}_1 \cdot \mathbf{k}_2) + \frac{4}{7}\frac{(\mathbf{k}_1 \cdot \mathbf{k}_2)^2}{k_1^2 k_2^2}. \tag{A.12}$$

Using the fact that in 3D the angular averages of α and β are respectively $\bar{\alpha} = 1$ and $\bar{\beta} = \frac{1}{3}$ we obtain:

$$\nu_2 \equiv 2\bar{F}_2 = 2\left[\frac{5}{7} + \frac{2}{7}\frac{1}{3}\right] = \frac{34}{21}; \qquad \mu_2 \equiv 2\bar{G}_2 = 2\left[\frac{3}{7} + \frac{4}{7}\frac{1}{3}\right] = \frac{26}{21}; \tag{A.13}$$

$$\nu_3 \equiv 6\bar{F}_3 = 6\left[\frac{7}{18}\left(\frac{17}{21} + \frac{13}{21}\right) + \frac{4}{18} \cdot \frac{1}{3} \cdot \frac{13}{21}\right] = \frac{682}{189}. \tag{A.14}$$

For 2D we use $\bar{\alpha} = 1$ and $\bar{\beta} = \frac{1}{2}$; in this case we have $\nu_2 \equiv 2\bar{F}_2 = \frac{12}{7}$, $\mu_2 \equiv 2\bar{G}_2 = \frac{10}{7}$,

Following recursion relation can be derived using Eq.(A.3) and Eq.(A.4) that is useful in evaluation of ν_n and μ_n results quoted above:

$$\nu_n = \sum_{m=1}^{n-1} \binom{n}{m} \frac{\mu_m}{(2n+3)(n-1)}\left[(2n+1)\nu_{n-m} + \frac{2}{3}\mu_{n-m}\right]; \tag{A.15}$$

$$\mu_n = \sum_{m=1}^{n-1} \binom{n}{m} \frac{\mu_m}{(2n+3)(n-1)}\left[3\nu_{n-m} + \frac{2}{3}n\mu_{n-m}\right]. \tag{A.16}$$

The perturbative bispectrum $B^{\rm PT}(\mathbf{k}_1,\mathbf{k}_2,\mathbf{k}_3)$ and trispectrum $T^{\rm PT}(\mathbf{k}_1,\mathbf{k}_2,\mathbf{k}_3,\mathbf{k}_4)$ take the following forms:

$$B^{\rm PT}(\mathbf{k}_1,\mathbf{k}_2,\mathbf{k}_3) = 2F_2(\mathbf{k}_1,\mathbf{k}_2)P(k_1)P(k_2) + 2 \text{ perm.}; \tag{A.17}$$

$$\begin{aligned} T^{\rm PT}(\mathbf{k}_1,\mathbf{k}_2,\mathbf{k}_3,\mathbf{k}_4) &= 4\left[F_2(\mathbf{k}_{13},-\mathbf{k}_1)F_2(\mathbf{k}_{13},\mathbf{k}_2)P(k_{13})P(k_2)P(k_2) + 11 \text{ perm.}\right] \\ &\quad +6\left[F_3(\mathbf{k}_1,\mathbf{k}_2,\mathbf{k}_3)P(k_1)P(k_2)P(k_3) + 3\text{perm.}\right] \end{aligned} \tag{A.18}$$

[[Few comments about the Lagrnagian and Eulerian perturbation theories are in order. In Eulerian PT the dynamics is formulated in a fixed Eulerian coordinate $\mathbf{x}$. The dynamical quantites δ and Θ are studied as a function of time. In Lagrangian theory the physical quantites of interests are studied along the particle trajectories and the perturbation here referes to perturbations in these trajectories. The ZA is the linear order in Lagrangian perturbation theory (LPT) [45]. The Eulerian perturbation theory is also referred to as standard perturbation theory (SPT).]]

B Perturbative Computation of the *Collapsed* Trispectrum

The aim in this section is to deduce the normalisation coefficient for the collapsed trispectrum and show it is same as given in Eq.(3.4). In the collapsed configuration the trispectrum includes contributions only from *snake* diagrams.

$$\begin{aligned} B_3(\mathbf{k}_1,\mathbf{k}_2,\mathbf{k}_3,\mathbf{k}_4) &= \langle\delta(\mathbf{k}_1)\delta^{(2)}(\mathbf{k}_2)\delta^{(2)}(\mathbf{k}_3)\delta(\mathbf{k}_4)\rangle_c + \langle\delta(\mathbf{k}_2)\delta^{(1)}(\mathbf{k}_2)\delta^{(2)}(\mathbf{k}_3)\delta(\mathbf{k}_4)\rangle_c \\ &\quad +\langle\delta(\mathbf{k}_1)\delta^{(2)}(\mathbf{k}_2)\delta^{(2)}(\mathbf{k}_4)\delta(\mathbf{k}_3)\rangle_c + \langle\delta(\mathbf{k}_2)\delta^{(1)}(\mathbf{k}_2)\delta^{(2)}(\mathbf{k}_4)\delta(\mathbf{k}_3)\rangle_c. \end{aligned} \tag{B.1}$$

Following Eq.(A.3) we express the second-order correction $\delta^{(2)}(\mathbf{k})$:

$$\delta^{(2)}(\mathbf{k}) = \delta_{\rm 3D}(\mathbf{k}-\mathbf{k}_{ab})\int\int \mathrm{F}_2(\mathbf{k}_a,\mathbf{k}_b)\delta^{(1)}(\mathbf{k}_a)\delta^{(1)}(\mathbf{k}_b)d^3\mathbf{k}_a\, d^3\mathbf{k}_b; \quad \mathbf{k}_{ab} = \mathbf{k}_a + \mathbf{k}_b \tag{B.2}$$

Here $\delta_{\rm 3D}$ is the 3D Dirac delta-function. Taking an ensemble average leads us to the following expression:

$$\langle\delta(\mathbf{k}_1)\delta^{(2)}(\mathbf{k}_2)\delta^{(2)}(\mathbf{k}_3)\delta(\mathbf{k}_4)\rangle_c = F_2(-\mathbf{k}_2,\mathbf{k}_{12})F_2(-\mathbf{k}_4,-\mathbf{k}_{12})P(\mathbf{k}_1)P(\mathbf{k}_{12})P(\mathbf{k}_4). \tag{B.3}$$

Combining the contributions from all four terms in Eq.(B.1):

$$\begin{aligned} B_3(\mathbf{k}_1,\mathbf{k}_2,\mathbf{k}_3,\mathbf{k}_4) &= P(\mathbf{k}_{12})\left[F_2(-\mathbf{k}_1,\mathbf{k}_{12})P(\mathbf{k}_1) + F_2(-\mathbf{k}_2,\mathbf{k}_{12})P(\mathbf{k}_2)\right] \\ &\quad \times\left[F_2(-\mathbf{k}_3,\mathbf{k}_{34})P(\mathbf{k}_3) + F_2(-\mathbf{k}_4,\mathbf{k}_{34})P(\mathbf{k}_4)\right]. \end{aligned} \tag{B.4}$$

We derive the expression for the collapsed trispectrum in this section. The results will be of practical use in estimation of covariance of local power spectrum estimates from survey sub-volumes. We start with definition of the local power spectrum in a sub-volume in Eq.(5.5). Next, we compute the covariance between the power spectrum at different mode k and k':

$$\begin{aligned} \langle\hat{P}(\mathbf{k},\mathbf{r}_{\rm L})\hat{P}(\mathbf{k}',\mathbf{r}_{\rm L})\rangle_c &= \frac{1}{V_L^2}\int\frac{d^3\mathbf{q}_1}{(2\pi)^3}\int\frac{d^3\mathbf{q}_2}{(2\pi)^3}\int\frac{d^3\mathbf{q}_1'}{(2\pi)^3}\int\frac{d^3\mathbf{q}_2'}{(2\pi)^3} \\ &\quad\times\langle\delta(\mathbf{k}-\mathbf{q}_1)\delta(-\mathbf{k}-\mathbf{q}_2)\delta(\mathbf{k}'-\mathbf{q}_1')\delta(-\mathbf{k}'-\mathbf{q}_2')\rangle \\ &\quad\times W_{\rm L}(\mathbf{q}_1)W_{\rm L}(\mathbf{q}_2)W_{\rm L}(\mathbf{q}_1')W_{\rm L}(\mathbf{q}_2')\exp[-i\mathbf{r}_{\rm L}\cdot(\mathbf{q}_{12}+\mathbf{q}_{12}')]. \end{aligned} \tag{B.5}$$

We use the following definition of collapsed trispectrum:

$$\begin{aligned}&\langle\delta(\mathbf{k}-\mathbf{q}_1)\delta(-\mathbf{k}-\mathbf{q}_2)\delta(\mathbf{k}-\mathbf{q}_1)\delta(-\mathbf{k}-\mathbf{q})\rangle_c\\&=(2\pi)^3\delta_{\rm D}(\mathbf{q}_{12}+\mathbf{q}'_{12})B_3[\mathbf{k}-\mathbf{q}_1,-\mathbf{k}+\mathbf{q}_1+\mathbf{q}_2,\mathbf{k}'-\mathbf{q}'_1,-\mathbf{k}'+\mathbf{q}'_1+\mathbf{q}'_2].\end{aligned}\tag{B.6}$$

In the collapsed limit the trispectrum takes the following form:

$$\lim_{\mathbf{q}_i\to 0} B_3[\mathbf{k}-\mathbf{q}_1,-\mathbf{k}+\mathbf{q}_1+\mathbf{q}_2,\mathbf{k}'-\mathbf{q}'_1,-\mathbf{k}'+\mathbf{q}'+\mathbf{q}'_3]\overset{\rm collapsed}{\approx} B_3[\mathbf{k},-\mathbf{k},\mathbf{k}',-\mathbf{k}'].\tag{B.7}$$

To simplify further, we express the 3D delta function $\delta_{3\rm D}$ in Eq.(B.6) as a convolution of two 3D delta function:

$$\delta_{3\rm D}(\mathbf{q}_{12}+\mathbf{q}'_{12})=\int d^3\mathbf{q}_3\,\delta_{3\rm D}(\mathbf{q}_{12}+\mathbf{q}_3)\,\delta_{3\rm D}(\mathbf{q}'_{12}-\mathbf{q}_3).\tag{B.8}$$

We use these $\delta_{3\rm D}$ functions to collapse the $\mathbf{q}_2$ and $\mathbf{q}'_2$ integrals:

$$\begin{aligned}&\langle\hat{P}(\mathbf{k},\mathbf{r}_{\rm L})\hat{P}(\mathbf{k}',\mathbf{r}_{\rm L})\rangle_c=\frac{1}{V_{\rm L}^2}\int\frac{d^3\mathbf{q}_1}{(2\pi)^3}\int\frac{d^3\mathbf{q}'_1}{(2\pi)^3}\int\frac{d^3\mathbf{q}_3}{(2\pi)^3}\\&\times B_3[\mathbf{k}-\mathbf{q}_1,-\mathbf{k}-\mathbf{q}_1-\mathbf{q}_3,\mathbf{k}',-\mathbf{k}'-\mathbf{q}'_1+\mathbf{q}_3]\\&\times W_L(\mathbf{q}_1)W_L(-\mathbf{q}_1-\mathbf{q}_3)W_L(\mathbf{q}'_1)W_L(\mathbf{q}_1-\mathbf{q}).\end{aligned}\tag{B.9}$$

After tedious but straightforward simplification, we get:

$$\begin{aligned}&B_3^{\rm coll}(\mathbf{k}_1,\mathbf{k}_2)\equiv B_3[\mathbf{k}-\mathbf{q}_1,-\mathbf{k}+\mathbf{q}_1+\mathbf{q}_3,\mathbf{k}'-\mathbf{q}'_1,-\mathbf{k}'+\mathbf{q}'_1-\mathbf{q}_3]\\&=P(k)P(k')P(q_3)\left[\frac{13}{7}+\frac{8}{7}\left(\frac{\mathbf{k}\cdot\mathbf{q}_3}{k\,q_3}\right)^2-\left(\frac{\mathbf{k}\cdot\mathbf{q}_3}{k\,q_3}\right)^2\frac{d\ln P(k)}{d\ln k}\right][\mathbf{k}\to\mathbf{k}'].\end{aligned}\tag{B.10}$$

The expression in the second bracket is obtained by replacing $\mathbf{k}$ with $\mathbf{k}'$. Next, we perform the angular integrals in the Fourier space.

$$\begin{aligned}&B_3^{\rm coll}(k,k')\equiv\int\frac{d^2\hat{\Omega}_{\mathbf{k}}}{4\pi}\int\frac{d^2\hat{\Omega}_{\mathbf{k}'}}{4\pi}\,B_3^{\rm coll}(\mathbf{k},\mathbf{k}')\\&=P(k)P(k')\sigma_L^2\left[\frac{68}{21}-\frac{1}{3}\frac{d\ln k^3P(k)}{d\ln k}\right][k\to k'].\end{aligned}\tag{B.11}$$

In our derivation, we have taken advantage of the Eq.(5.4). The factorisation of the expression in terms of products of two factors that depend either on $\mathbf{k}$ or $\mathbf{k}'$ allows us to perform the respective angular integration independently. Finally, assuming a local power-law for the power spectrum $P(k)\propto k^n$, we get:

$$\begin{aligned}&B_3^{\rm coll}(k,k')\equiv P(k)P(k')\,\sigma_L^2\,\left[2\nu_2-\frac{1}{3}(n+3)\right]\left[2\nu_2-\frac{1}{3}(n'+3)\right];\\&\frac{d\ln k^3P(k)}{d\ln k}=(n+3);\qquad\sigma_{\rm L}^2=\frac{1}{V_{\rm L}^2}\int d^3\mathbf{q}\,{\rm P}(k)\,W_{\rm L}^2(\mathbf{q}).\end{aligned}\tag{B.12}$$

The amplitude $\nu_2=34/21$ is defined in Eq.(A.14). As expected this numerical coefficient is identical to what was quoted for cumulant correlator in Eq.(3.4). The factorization ${\rm C}_{22}={\rm C}_{21}^2$

is a result of tree-level perturbation theory. Higher order contributions will be $\mathcal{O}(\sigma_L^4)$. For a reasonable big sub-volume such contribution will be negligible.

To recover the results derived in for HA valid in the non-linear regime §(A) we have to set $n = -3$ and identify $R_a = \nu_2^2$ eq.(5.14). The results derived here assumes a $\Omega = 1$ EdS cosmology. To probe residual dependence on cosmology we can follow the procedure outlined in §6.1. A similar derivations using $X_2(\mathbf{k}_1, \mathbf{k}_2)$ defined in Eq.(6.1) can be carried out which will replace the square bracket in Eq.(B.12) with appropriate Ω dependence of Eq.(6.4) or Eq.(6.5) (in case of 2D). This will also generalise the above result also to the case of Θ or for the case of ZA.

C Perturbative Computation of *Squeezed* Trispectrum

The aim of this section is to show that in the squeezed limit the normalisation coefficient takes same the form as Eq.(3.5). However in the squeezed configuration both star and snake diagrams contribute, thus making the calculations more involved.

Contributions From Snake Diagrams: The following six snake terms of the total twelve terms contribute in the leading order in the squeezed configuration:

$$\begin{aligned}\lim_{\mathbf{q}\to 0} B_3(\mathbf{q},\mathbf{k}_2,\mathbf{k}_3,\mathbf{k}_4) \overset{\text{snake}}{=} \lim_{\mathbf{q}\to 0} P(\mathbf{q})\Big\{ & P(\mathbf{k}_2)P(\mathbf{k}_4)\mathrm{F}_2(-\mathbf{k}_2,-\mathbf{k}_4)\left[\mathrm{F}_2(-\mathbf{q},\mathbf{k}_2)+\mathbf{k}_2\to\mathbf{k}_4\right] \\ & + P(\mathbf{k}_3)P(\mathbf{k}_4)\mathrm{F}_2(-\mathbf{k}_3,-\mathbf{k}_4)\left[\mathrm{F}_2(-\mathbf{q},\mathbf{k}_3)+\mathbf{k}_3\to\mathbf{k}_4\right]\Big\} \\ & + P(\mathbf{k}_2)P(\mathbf{k}_3)\mathrm{F}_2(-\mathbf{k}_3,-\mathbf{k}_2)\left[\mathrm{F}_2(-\mathbf{q},\mathbf{k}_2)+\mathbf{k}_2\to\mathbf{k}_3\right]\Big\}\delta_{3\mathrm{D}}(\mathbf{k}_{234}). \end{aligned} \tag{C.1}$$

$$B_2(\mathbf{k}_2,\mathbf{k}_3,\mathbf{k}_4) = \mathrm{F}_2^{\mathrm{sq}}(\mathbf{k}_1,\mathbf{k}_2)P(k_2)P(k_3) + \text{cyc.perm.}; \tag{C.2}$$

$$\mathrm{F}^{\mathrm{sq}}(\mathbf{k}_2,\mathbf{k}_4) = \mathrm{F}_2(\mathbf{k}_2,\mathbf{k}_4)\left[\mathrm{F}_2(-\mathbf{q},\mathbf{k}_2)+\mathbf{k}_2\to\mathbf{k}_4\right] \tag{C.3}$$

Thus the configuration from snake diagrams in the squeezed trispectrum takes the form of a bispectrum with a different vertex amplitude $\mathrm{F}_2^{\mathrm{sq}}$. For the hierarchical model the vertices are constant $F_2(\mathbf{k}_1,\mathbf{k}_2) = \nu_2$. In this limit the squeezed trispectrum takes simpler form and can be expressed in terms of the hierarchical bispectrum:

$$\lim_{\mathbf{q}\to 0} B_3(\mathbf{q},\mathbf{k}_2,\mathbf{k}_3,\mathbf{k}_4) = 2\nu_2\, P(q)\, B_2(\mathbf{k}_2,\mathbf{k}_3,\mathbf{k}_4) \tag{C.4}$$

In the limit $\{\mathbf{q},\mathbf{q}'\}\to 0$ in Eq.(C.1):

$$\lim_{\mathbf{q},\mathbf{q}'\to 0} B_3(\mathbf{q},\mathbf{q}',\mathbf{k},-\mathbf{k}) \overset{\text{snake}}{=} P(q)P(q')P(k)\{\mathrm{F}_2(\mathbf{q}_1,\mathbf{k})\mathrm{F}_2(-\mathbf{k},\mathbf{q}_2)+\mathbf{q}_1\leftrightarrow\mathbf{q}_2\}. \tag{C.5}$$

Contributions From Star Diagrams: The following four terms represent the star contributions to trispectrum:

$$B_3(\mathbf{k}_1,\mathbf{k}_2,\mathbf{k}_3,\mathbf{k}_4) \overset{\text{star}}{=} \langle\delta^{(3)}(\mathbf{k}_1)\delta(\mathbf{k}_2)\delta(\mathbf{k}_3)\delta(\mathbf{k}_4)\rangle_c + \text{cyc.perm.} \tag{C.6}$$

The expression for $\delta^{(3)}$ is expressed in terms of the kernel F_3 defined in Eq.(3.4):

$$\begin{aligned}\delta^{(3)}(\mathbf{k}) = \delta_{3\mathrm{D}}(\mathbf{k}-\mathbf{k}_{abc})\int d^3\mathbf{k}_a\,\delta(\mathbf{k}_a)\int d^3\mathbf{k}_b\,\delta(\mathbf{k}_b)\int d^3\mathbf{k}_c\,\delta(\mathbf{k}_c)\;F_3(\mathbf{k}_a,\mathbf{k}_b,\mathbf{k}_c); \\ \mathbf{k}_{abc} = \mathbf{k}_a+\mathbf{k}_b+\mathbf{k}_c.\end{aligned} \tag{C.7}$$

We need to consider the following configuration in the squeezed limit:

$$\lim_{\mathbf{q}_i\to 0} B_3(\mathbf{k}_1-\mathbf{q}_1,\mathbf{k}_2-\mathbf{q}_2,\mathbf{k}_3-\mathbf{q}_3,-\mathbf{q}_4)\delta_{3\rm D}(\mathbf{k}_{123})\delta_{3\rm D}(\mathbf{q}_{1234}); \\ \approx \lim_{\mathbf{q}_4\to 0} B_3(\mathbf{k}_1,\mathbf{k}_2,\mathbf{k}_3,-\mathbf{q}_4)\delta_{3\rm D}(\mathbf{k}_{123}). \tag{C.8}$$

The momentum-conserving Dirac's $\delta_{3\rm D}$ function in the Fourier domain $\delta_{3\rm D}(\mathbf{k}_{123})$ reduced to $\delta_{3\rm D}(\mathbf{k}_{123})$ in the squeezed limit $\mathbf{q}_4 \to 0$. Thus effectively reducing the trispectrum to a bispectrum. The terms that contribute are:

$$B_3(\mathbf{k}_1,\mathbf{k}_2,\mathbf{k}_3,-\mathbf{q}_4) \overset{\rm star}{=} P(q_4)\left[F_3(\mathbf{k}_1,\mathbf{k}_2,-\mathbf{q}_4)P(k_1)P(k_2)+\text{cyc.perm.}\right]. \tag{C.9}$$

Of the four terms listed in Eq.(C.6) only three survive as the contribution from the term $F_3(\mathbf{k}_1,\mathbf{k}_2,\mathbf{k}_3)$ vanishes due to the presence of the factor $\delta_{3\rm D}(\mathbf{k}_{123})$. In the limit $\{\mathbf{q},\mathbf{q}'\}\to 0$ in Eq.(C.6):

$$\lim_{\mathbf{q},\mathbf{q}'\to 0} B_3(\mathbf{q},\mathbf{q}',\mathbf{k},-\mathbf{k}) \overset{\rm star}{=} P(q)P(q')P(k)\left[F_3(\mathbf{q},\mathbf{q}',\mathbf{k})+F_3(\mathbf{q},\mathbf{q}',-\mathbf{k})\right]. \tag{C.10}$$

Total Contribution: Combining contributions from both *star* and *snake* topologies we arrive at the following expression:

$$B_3(\mathbf{q},\mathbf{k}_1,\mathbf{k}_2,\mathbf{k}_3) = P(q)\left[F_2'(\mathbf{k}_1,\mathbf{k}_2)P(k_1)P(k_2)+\text{cyc.perm.}\right]; \tag{C.11}$$

$$F_2'(\mathbf{k}_1,\mathbf{k}_2) \equiv \mathrm{F}_3(\mathbf{k}_1,\mathbf{k}_2,\mathbf{q}) + F_2(\mathbf{k}_1,\mathbf{k}_2)\left[F_2(-\mathbf{q},\mathbf{k}_1)+\mathbf{k}_1\to\mathbf{k}_2\right]. \tag{C.12}$$

For the hierarchical anasatz $\langle F_2\rangle = \nu_2$ and $\langle F_3\rangle = \nu_3$ and we get:

$$B_3(\mathbf{q},\mathbf{k}_1,\mathbf{k}_2,\mathbf{k}_3) = (\nu_3+2\nu_2^2)P(q)\left[P(k_1)P(k_2)+P(k_2)P(k_3)+P(k_1)P(k_3)\right]. \tag{C.13}$$

It thus takes an effective configuration of a bispectrum but with an amplitude determined by coefficients that determine the trispectrum.

Combining expressions from Eq.(C.5) and Eq.(C.10) we get in the limit $\{\mathbf{q},\mathbf{q}'\}\to 0$

$$\lim_{\mathbf{q},\mathbf{q}'\to 0} B_3(\mathbf{q},\mathbf{q}',\mathbf{k},-\mathbf{k}) = P(q)P(q')P(k)\Big[F_3(\mathbf{q},\mathbf{q}',\mathbf{k})+F_3(\mathbf{q},\mathbf{q}',-\mathbf{k}) \\ +\{F_2(\mathbf{q}_1,\mathbf{k})F_2(-\mathbf{k},\mathbf{q}_2)+\mathbf{q}_1\leftrightarrow\mathbf{q}_2\}\Big]. \tag{C.14}$$

C.1 Squeezed-limit Trispectrum

The integrated trispectrum (IT) $R_2(k)$ was derived in Ref.[54] [see Eq.(A.19)]:

$$R_3(k) \overset{\rm tree}{=} \frac{8420}{1323} - \frac{100}{63}\frac{d\ln P(k)}{d\ln k} + \frac{1}{9}\frac{k^2}{P(k)}\frac{d^2(k)}{dk^2}. \tag{C.15}$$

To arrive at this result we have used the following expressions $\langle\mu_1^2\rangle = \langle\mu_2^2\rangle = 1/3$ and $\langle\mu_{12}^2\rangle = 1/3$, $\langle\mu_1\mu_2\mu_{12}\rangle = 1/9$. We will next use the following expression:

$$\frac{k^2}{P(k)}\frac{d^2P(k)}{dk^2} = \left[\frac{d^2\ln P(k)}{d(\ln k)^2} - \frac{d\ln P(k)}{d\ln k} + \left(\frac{d\ln P(k)}{d\ln k}\right)^2\right]. \tag{C.16}$$

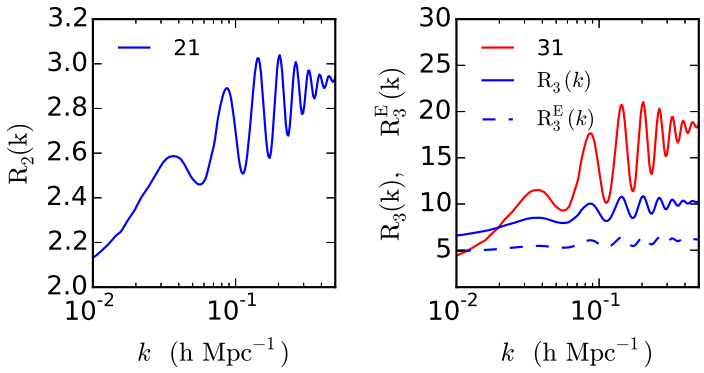

Figure 4: The 3D normalised cumulant correlators [defined in Eq.(3.4)-Eq.(3.5)] are compared with the coefficients R_2 in Eq.(C.19) and R_3 in Eq.(C.24)-Eq.(C.25) respectively. The left panel shows R_2 and the right panel depicts R_3 and R_3^E respectively along with C_{31}. Tree level perturbation theory is used in modelling of this quantities. The quantities R_2 and C_{21} are identical. However at third order the coefficients R_3(or its Eulerian counterpart R_3^E) and C_{31} are different.

To convert to Eulerian frame we use the following transformation in Eq.(4.1) of Ref.[54] :

$$R_3^{\rm E}(k) = R_3(k) - 2\, f_2\, R_2(k); \quad f_2 = \frac{17}{21}. \tag{C.17}$$

$$R_3^{\rm E}(k) = \frac{8420}{1323} - \frac{107}{63}\left[\frac{d\ln k^3P(k)}{d\ln k} - 3\right] + \frac{1}{9}\left[\frac{d\ln k^3P(k)}{d\ln k} - 3\right]^2 + \frac{1}{9}\frac{d^2\ln k^3P(k)}{d(\ln k)^2} - 2\frac{17}{21}\left(\frac{68}{21} - \frac{1}{3}\frac{d\ln k^3P(k)}{d\ln k}\right). \tag{C.18}$$

with

$$R_2(k) = \frac{68}{21} - \frac{1}{3}\frac{d\ln k^3P(k)}{d\ln k}. \tag{C.19}$$

For a power law power spectra we have $P(k) \propto k^n$ and we have $\frac{d\ln k^3P(k)}{d\ln k} = (n+3)$ and the term involving the second derivative vanishes.

For $n = -3$ we have for R_3 and R_3^E we have:

$$R_3 \overset{\rm n=-3}{=} \frac{8420}{1323} + \frac{107}{21} + 1 = \frac{16484}{1323}; \tag{C.20}$$

$$R_3^{\rm E} \overset{\rm n=-3}{=} R_3 - 2\cdot\frac{17}{21}\cdot\frac{68}{21} = \frac{1364}{189}. \tag{C.21}$$

Using HA we recover:

$$\lim_{\mathbf{q},\mathbf{q}'\to 0} B_3[\mathbf{q},\mathbf{q}',\mathbf{k},-\mathbf{k}] \overset{\rm HA}{=} (4\nu_2^2 + 2\nu_3)P(q)P(q')P(k). \tag{C.22}$$

This is consistent with Eq.(3.5) that defines the cumulant correlator C_{31}.

However, using PT kernels the results in Ref.[54] are equivalent to (for $n = -3$ in 3D):

$$\lim_{\mathbf{q},\mathbf{q}'\to 0} B_3[\mathbf{q},\mathbf{q}',\mathbf{k},-\mathbf{k}] \stackrel{\rm PT}{=} (2\nu_2^2 + 2\nu_3)P(q)P(q')P(k). \tag{C.23}$$

We get Eq.(C.20) if we use the squeezed limit in Eq.(C.23).

In case of a locally power-law spectrum with arbitrary index n we have:

$$R_3(k) \stackrel{\rm tree}{=} \frac{16484}{1323} - \frac{3129}{1323}(n+3) + \frac{147}{1323}(n+3)^2. \tag{C.24}$$

The Eulerican counterpart takes the following the expression:

$$R_3^{\rm E}(k) \stackrel{\rm tree}{=} \frac{1364}{189} - \frac{345}{189}(n+3) + \frac{1}{9}(n+3)^2. \tag{C.25}$$

These expressions are plotted in Figure 4 along with their kurt-spectra counterpart defined in Eq.(3.5).